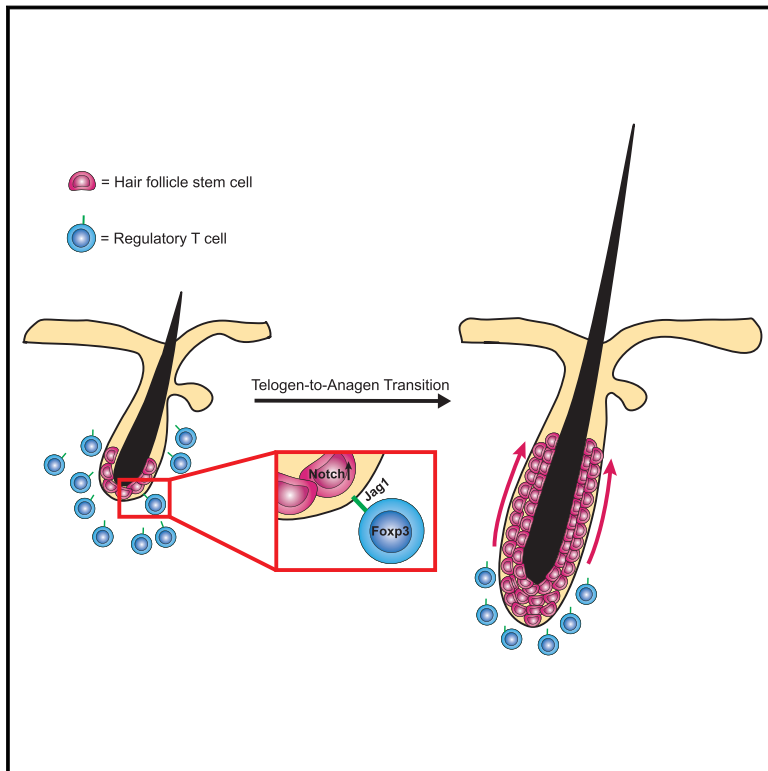# Cell

Regulatory T Cells in Skin Facilitate Epithelial Stem Cell Differentiation

Graphical Abstract

Authors

Niwa Ali, Bahar Zirak,
Robert Sanchez Rodriguez, ...,
George Cotsarelis, Abul K. Abbas,
Michael D. Rosenblum

Correspondence

michael.rosenblum@ucsf.edu

In Brief

Localized regulatory T cells (Tregs) regulate the hair follicle cycle by driving Notch-dependent stem cell proliferation and differentiation.

Highlights

- Treg activation in skin closely correlates with the HF cycle

- Tregs localize to HFSCs and play a major role in HF regeneration

- Tregs facilitate HFSC proliferation and differentiation to initiate HF cycling

- Treg expression of Jagged 1 is required for efficient hair regeneration

CellPress

Regulatory T Cells in Skin Facilitate Epithelial Stem Cell Differentiation

Niwa Ali,[1,3] Bahar Zirak,[1] Robert Sanchez Rodriguez,[1] Mariela L. Pauli,[1] Hong-An Truong,[1] Kevin Lai,[1] Richard Ahn,[1] Kaitlin Corbin,[2] Margaret M. Lowe,[1] Tiffany C. Scharschmidt,[1] Keyon Taravati,[1] Madeleine R. Tan,[1] Roberto R. Ricardo-Gonzalez,[1] Audrey Nosbaum,[1] Marta Bertolini,[4] Wilson Liao,[1] Frank O. Nestle,[3] Ralf Paus,[5] George Cotsarelis,[6] Abul K. Abbas,[2] and Michael D. Rosenblum[1,7,*]

[1]Department of Dermatology
[2]Department of Pathology
University of California, San Francisco, San Francisco, CA 94143, USA
[3]Cutaneous Medicine Unit, St. John's Institute of Dermatology, King's College London, London WC2R 2LS, UK
[4]Department of Dermatology, University of Muenster, 48149 Muenster, Germany
[5]Centre for Dermatological Research, University of Manchester & NIHR Manchester Biomedical Research Centre, Manchester M13 9PL, UK
[6]Department of Dermatology, Perelman School of Medicine, University of Pennsylvania, Philadelphia, PA 19104, USA
[7]Lead Contact
*Correspondence: michael.rosenblum@ucsf.edu
http://dx.doi.org/10.1016/j.cell.2017.05.002

SUMMARY

The maintenance of tissue homeostasis is critically dependent on the function of tissue-resident immune cells and the differentiation capacity of tissue-resident stem cells (SCs). How immune cells influence the function of SCs is largely unknown. Regulatory T cells (Tregs) in skin preferentially localize to hair follicles (HFs), which house a major subset of skin SCs (HFSCs). Here, we mechanistically dissect the role of Tregs in HF and HFSC biology. Lineage-specific cell depletion revealed that Tregs promote HF regeneration by augmenting HFSC proliferation and differentiation. Transcriptional and phenotypic profiling of T$_{regs}$ and HFSCs revealed that skin-resident Tregs preferentially express high levels of the Notch ligand family member, Jagged 1 (Jag1). Expression of Jag1 on Tregs facilitated HFSC function and efficient HF regeneration. Taken together, our work demonstrates that Tregs in skin play a major role in HF biology by promoting the function of HFSCs.

INTRODUCTION

Forkhead box P3 (FOXP3)-expressing regulatory T (Treg) cells are a specialized subset of CD4$^+$ T cells that play a major role in establishing and maintaining immune tolerance. In the steady-state, the majority of these cells reside in primary and secondary lymphoid organs. However, subsets of Tregs stably reside in specific peripheral tissues, and an emerging body of literature suggests that tissue-resident Tregs have specialized functions that are unique to the tissues in which they reside. In visceral adipose tissue, Tregs express the peroxisome proliferator-activated receptor-γ, enabling them to function in lipid and glucose metabolism (Cipolletta et al., 2012). In addition, Tregs in muscle and lung express high levels of the epidermal growth

factor ligand, amphiregulin, conferring the ability to mediate tissue protection and maintain barrier integrity (Arpaia et al., 2015; Burzyn et al., 2013; Villalta et al., 2014).

Both murine and human skin contain a large number of tissue-resident Tregs (Clark et al., 2006; Sanchez Rodriguez et al., 2014; Scharschmidt et al., 2015). However, the function of these cells in this tissue is only beginning to be elucidated. Early in neonatal life, a wave of highly activated Tregs accumulates in skin and plays a major role in establishing immune tolerance to skin commensal microbes (Scharschmidt et al., 2015). In adult life, a subset of Tregs in skin facilitates wound healing through increased expression of the epidermal growth factor receptor (EGFR) (Nosbaum et al., 2016). Tregs that reside in skin predominantly localize around hair follicles (HFs) (Chow et al., 2013; Gratz et al., 2013; Sanchez Rodriguez et al., 2014). Hair follicles are highly specialized organelles that are in a perpetual state of growth and regeneration. In addition to Tregs, a major epithelial stem cell (SC) population localizes to HFs (HFSCs) (Blanpain and Fuchs, 2009). These cells play an indispensable role in HF regeneration and repair of the epidermal barrier after injury (Ito et al., 2005). Interestingly, several studies link Tregs with HF biology. Genome-wide association studies in alopecia areata (AA), a disorder of HF regeneration, have revealed single nucleotide polymorphisms in genes involved in the differentiation and function of Tregs, including interleukin (IL)-2, the high-affinity IL-2 receptor alpha (CD25), CTLA-4, Eos (IKZF4), and Foxp3 (Petukhova et al., 2010). In addition, pharmacologic augmentation of Tregs in humans with low-dose IL-2 was highly efficacious in treating AA (Castela et al., 2014). Despite these associations, a functional link between Tregs and HFs has yet to be established.

Given that Tregs in skin localize to HFs, polymorphisms in genes intimately associated with Treg function are increased in patients with AA, and Treg enhancement promotes hair regeneration in this disease, we sought to determine whether Tregs play a functional role in HF biology. Immunophenotypic profiling revealed that Treg numbers and activation in skin tightly correlate with specific phases of the HF cycle. Lineage-specific depletion of these cells resulted in a marked attenuation of HF
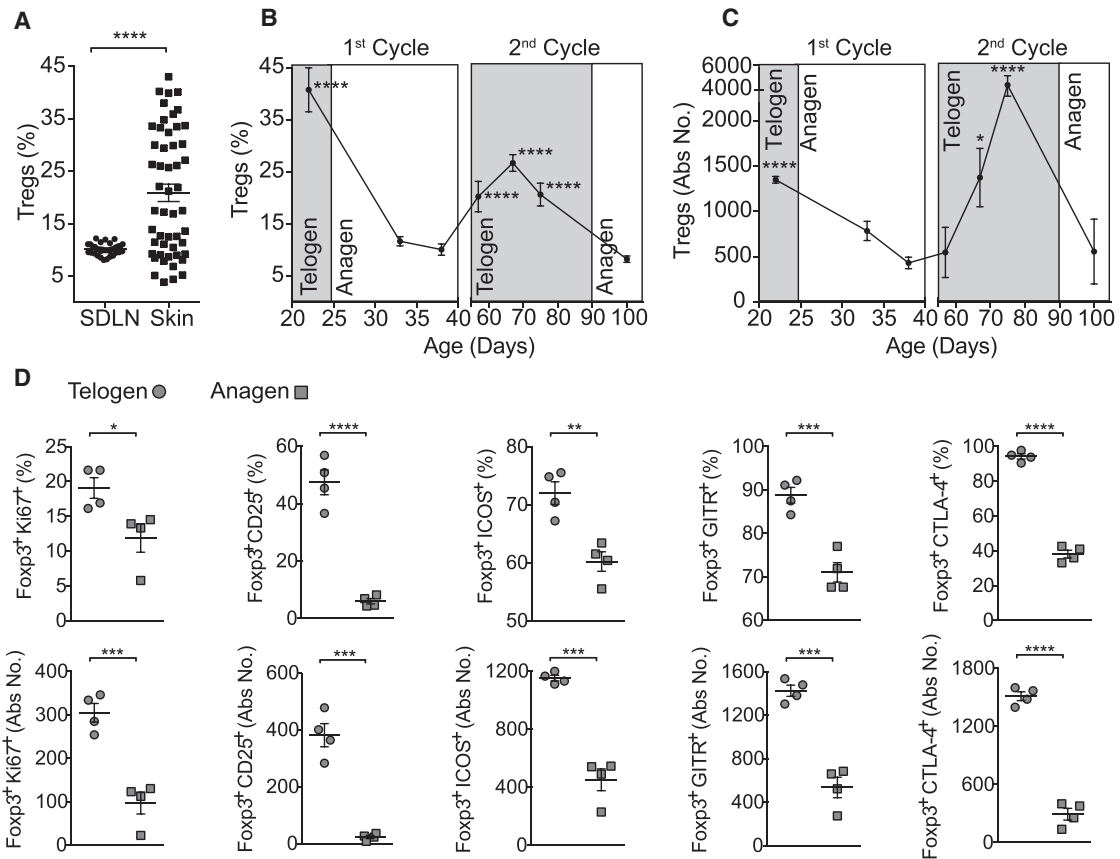
Figure 1. Treg Accumulation and Activation in Skin Correlates with the HF Cycle

(A) Treg cell abundance in skin draining lymph nodes (SDLNs) and skin of adult 4- to 14-week-old WT mice as measured by flow cytometry. Pre-gated on live $CD45^+CD3^+CD4^+$ cells.

(B and C) Flow cytometric profiling of Treg (B) frequency and (C) absolute numbers from dorsal skin of C57BL/6 mice at specific stages of the synchronous HF cycle (n = 5–12 mice per time point). Shaded areas represent telogen phase and unshaded areas represent anagen phase. Treg-associated activation markers were assessed: CD25, ICOS, Ki67, CTLA-4, and GITR.

(D) Summary of percent and absolute cell number (Abs No.) quantification of Treg activation marker expression in telogen and anagen skin. One representative experiment of three is shown. Data are mean ± SEM. *p < 0.05, **p < 0.01 ***p < 0.001, ****p < 0.0001; one-way ANOVA first telogen versus first anagen and second telogen versus second anagen (B and C), Student's unpaired t test (D).

See also Figure S1.

regeneration. Mechanistically, we found that Tregs promote HF cycling by enhancing the activation and differentiation of HFSCs. An unbiased discovery approach revealed that Tregs in skin express high levels of the Notch ligand, Jagged 1 (Jag1), and signaling through the Notch pathway is a major mechanism by which Tregs promote HFSC function. Our studies reveal a mechanistic link between skin-resident Tregs and HFSCs that is critical for tissue function.

RESULTS

Highly Activated Tregs Accumulate in Telogen Skin

Hair follicles in mammalian skin undergo bouts of regeneration, cycling between highly synchronized phases of quiescence (telogen) and growth (anagen), ultimately resulting in the generation of a newly formed hair shaft (Müller-Röver et al., 2001). To test the hypothesis that Tregs play a functional role in HF biology, we began by performing comprehensive immune profiling of Tregs in murine skin at specific stages of the synchronous HF cycle (Müller-Röver et al., 2001). The proportion of $CD4^+Foxp3^+$ Tregs in skin-draining lymph nodes (SDLNs) of adult C57BL/6 mice showed little variability (Figure 1A). In contrast, the accumulation of Tregs in dorsal skin was highly variable; however, this variance tightly correlated with HF cycling (Figures 1A–1C and S1A). Tregs were significantly more abundant in the telogen phase of the HF cycle when compared to anagen (Figures 1B and S1A). To ensure that these results were not an artifact of the tissue digestion required for flow cytometric analysis and to confirm that Tregs were accumulating around HFs, we quantified Tregs during telogen and anagen phases of the HF cycle by immunofluorescent microscopy. These studies revealed a ∼3-fold higher accumulation around HFs in telogen skin relative to anagen skin, confirming our flow cytometric results (Figures S1B and S1C). While Tregs are uniquely more abundant in
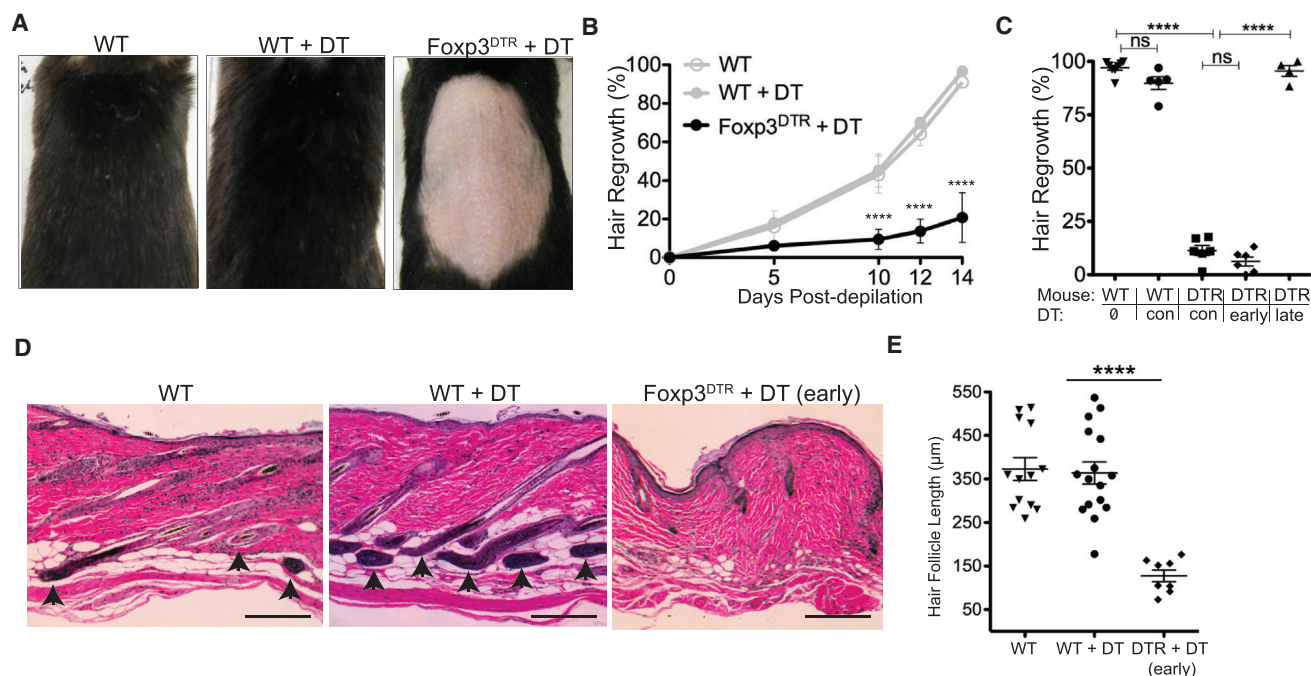
Figure 2. Tregs Are Required for Hair Regeneration

(A and B) Foxp3[DTR] mice or control WT were treated with DT on days −2, −1, and depilated on day 0 to induce anagen. DT administration was continued from Day 1 and then every other day until the termination of the experiment at day 14. (A) Representative photos and (B) kinetics of hair regrowth in WT and Treg-depleted (Foxp3[DTR]) mice (n = 3–4 mice per group). Tregs were depleted either up to day 4 (early), from day 7 onward (late) or constitutively (con) throughout the experimental period.

(C) Hair regrowth at day 14 in WT and Foxp3[DTR] mice with DT treatments as indicated.

(D) Representative H&E staining of skin from WT and Foxp3[DTR] mice on day 14. Arrows indicate anagen HF extension into dermal adipose. Scale bars, 100 μm.

(E), Quantification of HF length on day 14. Data are mean ± SEM. ****$p < 0.0001$, ns, not significant; one-way ANOVA (B, C, and E). Foxp3[DTR] + DT versus WT + DT (B).

See also Figure S2.

telogen skin relative to anagen skin, Foxp3 negative T effector cells (Teff) and CD8^{+} T cells show an inverse relationship to Tregs, and dermal gamma-delta T cells show little fluctuation with the HF cycle (Figure S1D). In addition, the proliferative index and activation state of skin Tregs (as evidenced by expression of Ki67, CD25, ICOS, GITR, and CTLA-4) correlated with stage of the HF cycle, as Tregs displayed a highly activated phenotype in telogen skin relative to anagen skin (Figures 1D and S1E). Taken together, these results suggest that Treg abundance and activation in skin tightly correlate with the HF cycle, with highly activated Tregs preferentially accumulating around HFs during late telogen.

Regulatory T Cells Are Required for Hair Regeneration

Given that both Treg abundance and activation correlated with HF stage, we sought to determine whether these cells play a functional role in HF cycling. To do so, we employed a well-established model of depilation-induced HF regeneration (Müller-Röver et al., 2001). In this model, mice with dorsal skin HFs in telogen are depilated to remove hair shafts. This treatment rapidly initiates the telogen-to-anagen transition homogenously across the entire depilated dorsum (i.e., anagen induction) and thus begins the process of hair regeneration. To determine if Tregs play a role in this process, we utilized mice

transgenic for the diphtheria toxin receptor under the control of the Foxp3 promoter (Foxp3[DTR]) (Kim et al., 2007). These mice allow for robust depletion of Tregs following administration of Diphtheria toxin (DT). Importantly, Tregs begin to repopulate lymph nodes and peripheral tissues soon after the last DT treatment, permitting the study of transient Treg loss at specific times during HF regeneration (Kim et al., 2007). We monitored these mice for dorsal skin pigmentation, which is the earliest clinical sign of anagen entry (Müller-Röver et al., 2001), as well as clinical hair regrowth. Ablation of Tregs markedly reduced anagen induction and subsequent hair regrowth when compared to control wild-type (WT) mice treated with or without DT (Figures 2A, 2B, S2A, and S2B). Whereas control mice had efficient anagen induction and completed hair regrowth by 14 days post-depilation, mice depleted of Tregs showed a marked diminution of anagen induction and had <20% hair regrowth at 14 days (Figures 2A, 2B, and S2A–S2D).

In these initial experiments, Tregs were continually depleted (i.e., DT administered every 2 days for 14 days). Because a major function of T_regs is to suppress inflammation, mice deficient in these cells for prolonged periods of time develop multi-organ autoimmunity (Kim et al., 2007). Thus, we set out to determine whether attenuation of HF cycling in the absence of Tregs was a result of prolonged systemic inflammation. In
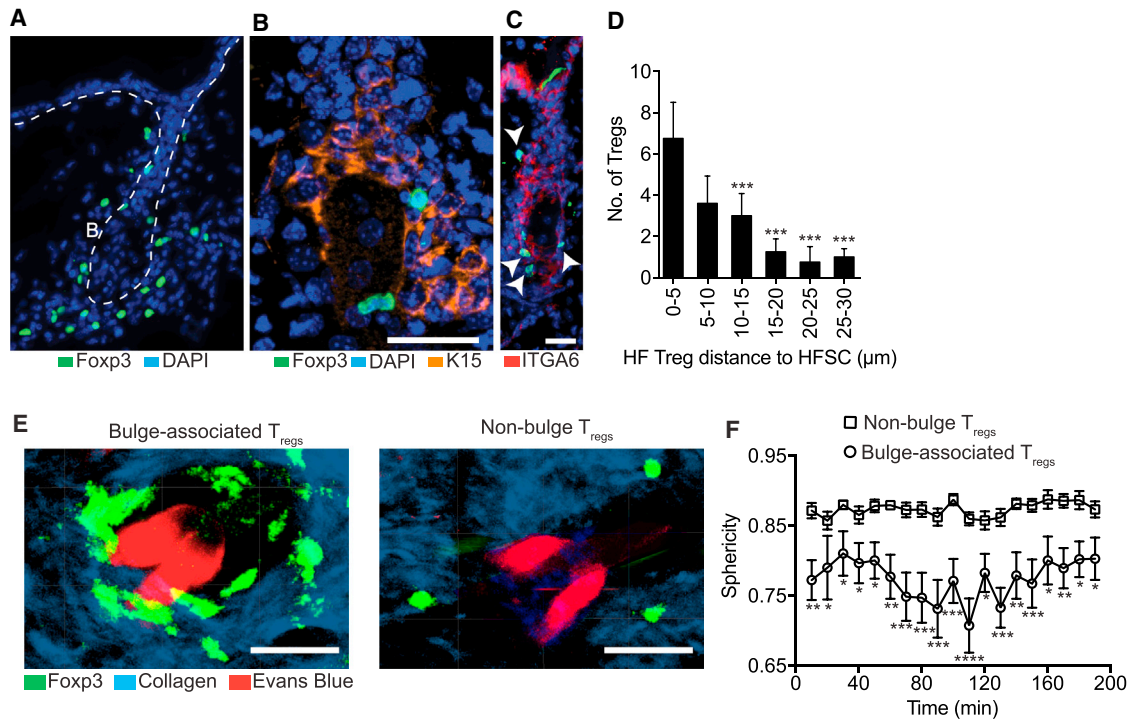
Figure 3. Tregs in Skin Preferentially Reside in Close Approximation to HFSCs

(A) Representative immunofluorescent image of Foxp3^{+} Tregs in telogen skin of Foxp3[GFP] reporter mice. Dashed line indicates outline of HF. "B" indicates bulge region.

(B and C) Treg cell co-staining with (B) Keratin-15 (K15) and (C) integrin-alpha 6 (ITGA6).

(D) Quantification of follicular Treg distance to bulge HFSCs. Data are combined counts from greater than ten sections.

(E) Maximal intensity projection profiles of bulge-associated and non-bulge-associated Tregs from intravital imaging of Foxp3[GFP] mice compiled from images recorded every 10 min during a 200-min time lapse. HF vasculature is labeled with Evans blue dye (red).

(F) Quantification of cell sphericity between bulge-associated and non-bulge-associated Tregs during a 200-min time lapse. Scale bars, 50 μm. Data are mean ± SEM. $*p < 0.05$, $**p < 0.01$ $***p < 0.001$, $****p < 0.001$; one-way ANOVA, 0–5 μm versus all other groups (D). Two-way ANOVA, bulge- versus non-bulge Tregs at each respective time point (F). One representative experiment of three with n = 3 mice total.

See also Figure S3 and Movies S1 and S2.

addition, we wanted to precisely define a potential "window" of time for Treg requirement in HF cycling. To do so, we treated WT or Foxp3[DTR] mice with DT "early" after depilation (up to 4 days post-depilation), "late" after depilation (starting at 7 days post-depilation), or throughout the entire 14-day period of hair regeneration. Transient depletion of Tregs early after depilation fully recapitulated the attenuation of HF regeneration observed with constant Treg depletion. In contrast, late Treg depletion had no effect on hair regrowth (Figures 2C, S2C, and S2D). Histologic examination of skin showed a marked diminution of anagen HFs in "early" Treg-depleted mice. Whereas HFs in control mice displayed an elongated phenotype extending deep into the dermal adipose (indicative of anagen induction) (Müller-Röver et al., 2001), HFs from Treg-depleted mice were significantly shorter in length and failed to extend beyond the superficial dermis (Figures 2D, 2E, S2E, and S2F). Consistent with these findings, mice that lack all T cells (Rag2^{−/−}) have a significant delay in anagen induction capacity in response to depilation-induced hair regeneration, as well as during the natural synchronous HF cycle (Figures S2G–S2J). Taken together, these results indicate that Tregs

play a major role in facilitating HF regeneration by promoting the telogen-to-anagen transition.

Regulatory T Cells in Skin Preferentially Localize to the HFSC Niche

Hair follicle stem cells play a major role in HF regeneration (Blanpain and Fuchs, 2009). The transition of telogen HFs to anagen HFs is mediated by the activation, proliferation and differentiation of HFSCs (Blanpain et al., 2006; Morris et al., 2004; Trempus et al., 2003). Because Tregs in skin localize to HFs (Chow et al., 2013; Gratz et al., 2013; Sanchez Rodriguez et al., 2014) and facilitate the telogen-to-anagen transition, we set out to determine if Tregs in skin co-localize with HFSCs. Immunofluorescence microscopy of dorsal skin of Foxp3[GFP] reporter mice (Lin et al., 2007) revealed that Tregs predominantly reside proximal to the lower portions of telogen HFs, clustering around the bulge region (Figure 3A), a well-established niche for HFSCs (Morris et al., 2004; Trempus et al., 2003). Co-staining of cytosolic expressed GFP with markers of bulge resident SCs (Morris et al., 2004), Keratin-15, and ITGA6, revealed a sub-population of bulge-associated Tregs in close association with HFSCs

(Figures 3B, 3C, and S3). Quantification of Foxp3-GFP$^+$ Tregs within 30 μm of follicular epithelium demonstrated that the majority of follicular Tregs reside within 0–5 μm of bulge HFSCs (Figure 3D).

To determine the dynamic behavior of Tregs in skin with high hair density (i.e., dorsal skin), we established a non-invasive vacuum suction approach for live intravital 2-photon imaging of Tregs in dorsal skin of Foxp3^{GFP} reporter mice. This technique was adapted from approaches utilized in other tissues (Boldajipour et al., 2016; Broz et al., 2014; Headley et al., 2016; Lin et al., 2007; Lindsay et al., 2015; Looney et al., 2011; Sano et al., 2016; Vinegoni et al., 2012). Evans blue dye was utilized to ensure all intravascular Tregs were excluded while all cells located in the extravascular space were included for analysis. Utilizing this system, we observed that bulge-associated Tregs differ markedly with respect to shape and behavior when compared to Tregs found >20 μm away from follicular epithelium. Bulge-associated Tregs displayed a more amoeboid cell morphology with increased protrusive activity (Figure 3E; Movies S1 and S2). This differential cell shape was quantified in individual skin Tregs by applying a measure of relative sphericity (Matheu et al., 2013; Zaid et al., 2014). Cells that are in contact with other cells typically have characteristic dynamic behavior. Specifically, cell-to-cell contacts alter the shape of cells such that they are no longer spherical (Lecuit and Lenne, 2007). When compared to non-bulge Tregs, the sphericity of bulge-associated Tregs was significantly lower at all time points analyzed (Figure 3F). While this parameter is not a specific measure of Treg function, our findings indicate that Tregs in and around the HF niche are more dynamically active when compared to Tregs found outside this region. Taken together with images obtained by static immunofluorescence microscopy, these results suggest that Tregs are highly active in the bulge region of the HF and have the potential to communicate with bulge-associated HFSCs.

## Regulatory T Cells Promote HFSC Proliferation and Differentiation

Given that HFs from Treg-depleted mice failed to regenerate, Tregs reside in the bulge region of the HF in close association with HFSCs, and activation of HFSCs is necessary and required for HF regeneration, we tested whether Tregs mediate their effects by influencing the function of HFSCs. Upon anagen induction, HFSCs are activated, begin to proliferate, and eventually differentiate to form all cell lineages of the newly generated HF (Blanpain et al., 2006; Morris et al., 2004; Trempus et al., 2003). Because Tregs function early to facilitate anagen induction, we set out to determine their influence on HFSC activation during the telogen-to-anagen transition. To do so, we utilized a previously established flow cytometric approach to delineate HFSCs (Nagao et al., 2012). Epidermal cell suspensions were prepared from dorsal skin and stained for CD45, Sca-1, EpCAM, CD34, and integrin α6 (ITGA6). Bulge HFSCs were defined as CD45^{neg}Sca-1^{neg}EpCAM^{low}CD34^{high} cells (Figure 4A). High levels of ITGA6 expression on this population distinguishes basal bulge residing HFSCs from those in the suprabasal layer (Trempus et al., 2003). Analysis of mid-telogen WT skin confirmed the presence of quiescent bulge-resident HFSCs (Cotsarelis et al.,

1990), as evidenced by lack of expression of the proliferative marker Ki67 (Figures 4B and 4C). Consistent with previous reports, HFSC activation closely followed depilation-induced anagen induction (Chen et al., 2012), with an increased percentage of HFSCs expressing Ki67 early after depilation (Figures 4B and 4C). Induction of HFSC proliferation was significantly attenuated in mice transiently depleted of Tregs in the early window of time after depilation (Figures 4B and 4C). This proliferative defect appeared to be selective for the bulge HFSC compartment, as no difference in Ki67 expression was observed in non-bulge keratinocytes between Treg-sufficient and Treg-depleted mice (Figure 4D). Absolute cell numbers of HFSCs were unchanged between all treatment groups, suggesting that HFSCs are not DT-sensitive or directly depleted in Foxp3^{DTR} mice (Figure S4A). Absence of Ki67 in the bulge region of the HF in Treg-depleted mice was confirmed by histological staining of dorsal skin sections (Figure S4B).

To determine if T$_{regs}$ play a similar role in steady-state-mediated HFSC activation during the natural telogen-to-anagen transition, we transiently administered DT or PBS (vehicle control) to Foxp3^{DTR} mice to deplete Tregs during first telogen from postnatal day 21 (P21) to P24. Relative to littermate controls, DT-treated Foxp3^{DTR} mice fail to enter first anagen as evidenced by a lack of dorsal skin pigmentation and significantly diminished proliferative capacity of HFSCs (Figures S4C–S4E). While the absolute number of CD34$^+$ HFSCs was equivalent, the proportion and absolute number of proliferating Ki67$^+$ HFSCs were significantly lower in Treg-depleted mice (Figures S4F–S4H). These data provide evidence that Tregs play a role in promoting the telogen-to-anagen transition during the natural HF cycle.

To investigate the in vivo frequency of proliferative HFSCs, we performed short-term nucleotide labeling via injection of 5-ethynyl-2′-deoxyuridine (EdU) at day 3 post-anagen entry and measured incorporation into HFSCs 24 hr later. While Treg-sufficient mice efficiently incorporated EdU, the median fluorescence intensity (MFI) of HFSCs in Treg-deficient mice was significantly less (Figures S4I and S4J). These results indicate that in the absence of Tregs, HFSCs are unable to undergo multiple rounds of proliferation during this 24-hr chase period. These findings are consistent with experiments showing reduced Ki67$^+$ HFSCs by flow cytometry (Figures 4B and 4C).

To elucidate if Tregs influence HFSC differentiation, we performed whole transcriptome RNA sequencing (RNA-seq) of bulge HFSCs. Lineage tracing studies in the SC niche have identified a role for ITGA6-expressing basal cell progenitors and their progeny in adopting a HF fate (Ito et al., 2005; Jaks et al., 2008; Levy et al., 2005; Morris et al., 2004; Tumbar et al., 2004). We therefore analyzed CD34$^+$ITGA6^{high} basal bulge HFSCs purified from Treg-sufficient and Treg-depleted mice 4 days post-depilation. Consistent with our Ki67 flow cytometric data, HFSC from Treg-depleted mice showed a significant reduction in genes associated with cell proliferation (Table S1). In addition, these HFSCs also showed a reduction in genes associated with the differentiation of HFSCs to keratinocyte lineages, including Bgn, Bnc1, Cks2, Hmgn3, Gdf10, and Sox4 (Figure 4E) (Lowry et al., 2005). Collectively, these results suggest that a major mechanism by which Tregs mediate HF cycling is by promoting the activation and differentiation of bulge HFSCs.
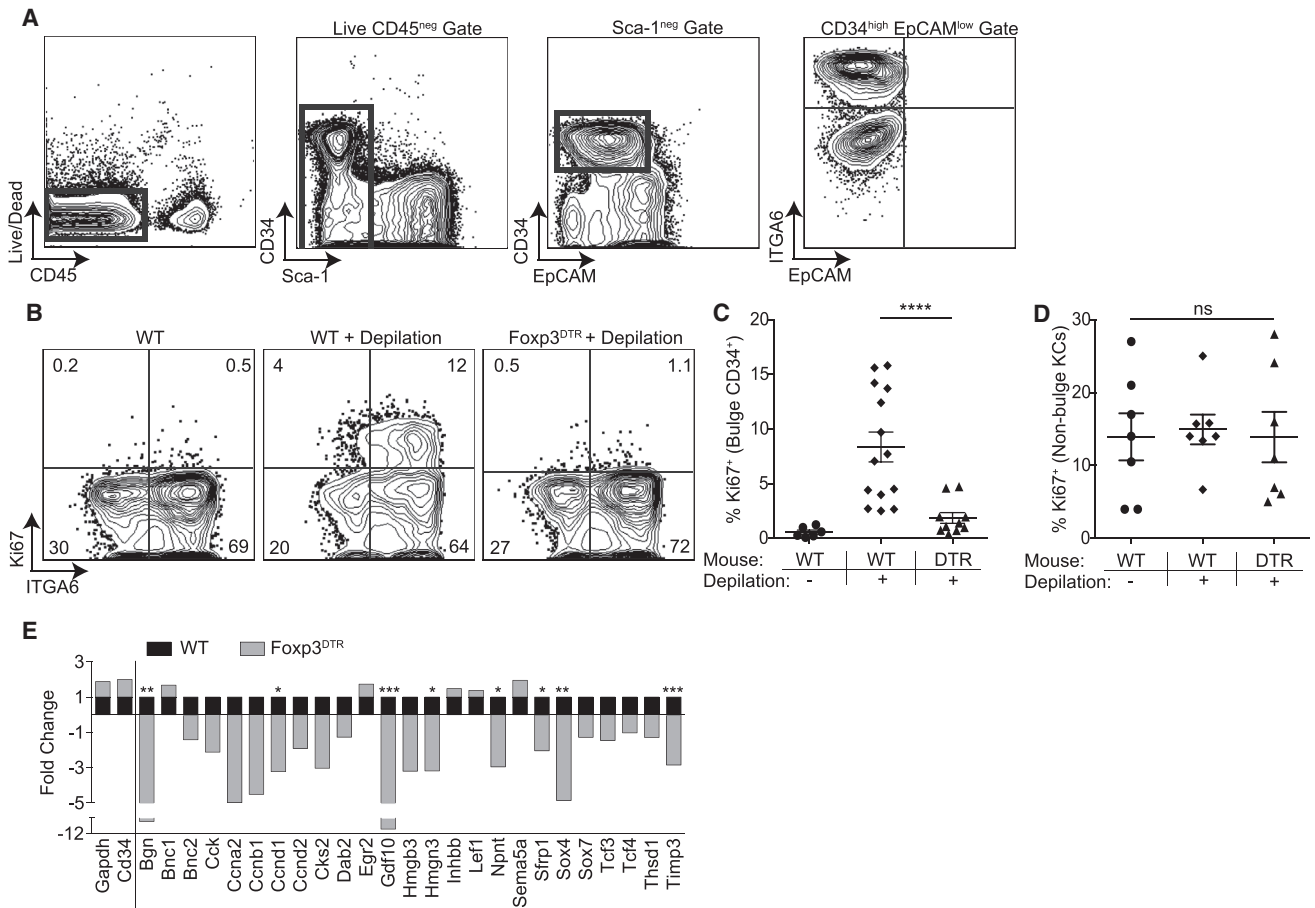
Figure 4. Tregs Are Required for HFSC Proliferation and Differentiation

(A) Flow cytometric gating strategy to identify CD34$^+$ integrin $\alpha6^{high}$ (ITGA6) bulge HFSCs. Foxp3^{DTR} mice or control mice were treated with DT on days -2, -1, depilated on day 0 to induce anagen and DT administered again on days 1 and 3 (i.e., early regimen).

(B) Representative flow cytometric plots of Ki67 expression in bulge HFSCs between WT and Foxp^{DTR} mice 4 days after depilation.

(C and D) Flow cytometric quantification of Ki67$^+$ (C) bulge HFSCs and (D) non-bulge keratinocytes 4 days after depilation. RNA sequencing was performed on fluorescence-activated cell sorting (FACS) purified bulge HFSCs at day 4 post-depilation from control (WT) or Treg-depleted (Foxp3^{DTR}) mice.

(E) Fold change in HFSC differentiation genes in WT and Foxp^{DTR} mice, expressed as fold change relative to WT (where a value of 1 = no change). Genes to the left of the solid line represent control genes. Significance values are calculated based on transcript expression level. Data are mean ± SEM. *p < 0.05, **p < 0.01 ***p < 0.001, ****p < 0.0001, ns, no significant difference. One-way ANOVA (C and D); RNA-seq differential expression analysis, WT versus Foxp3^{DTR} for each respective gene (E).

See also Figure S4 and Table S1.

Transient Treg Depletion Results in Minimal Skin Inflammation

We next set out to determine the cellular and molecular mechanisms by which Tregs influence HFSC function. Because a major mechanism by which Tregs mediate their effects is through suppression of inflammation, we first set out to define the inflammatory milieu in skin after transient Treg depletion "early" after depilation. Surprisingly, classic hallmarks of skin inflammation, such as epidermal hyperplasia and immune cell infiltrate, were not significantly different between control mice and mice transiently depleted of Tregs (Figures 2D and 5A–5C). Consistent with these findings, flow cytometric quantification of the absolute numbers of dermal γδ T cells, dendritic epidermal T cells, cytotoxic CD8$^+$ T cells, CD4$^+$Foxp3$^-$ T effector cells, dendritic cells, neutrophils, and macrophages revealed no differences be-

tween Treg-depleted and Treg-sufficient mice (Figure 5D). In addition, skin effector T cell production of interleukin (IL)-22, interferon-gamma, IL-17, and tumor necrosis factor-alpha were similar between control and transient Treg-depleted mice (Figures 5E–5G and S5). To functionally determine if inflammatory cells play a role in Treg-mediated activation of HFSCs, we co-depleted Tregs with specific immune cell subsets to determine if HFSC function could be rescued in the absence of Tregs. HFSC proliferation was not restored following co-depletion of Tregs with CD4$^+$ T cells, CD8$^+$ T cells, Gr-1 expressing neutrophils, or CD11c-expressing myeloid cells (Figure 5H). In addition, both antibody neutralization and genetic deletion of the interferon-γ pathway, a major effector cytokine suppressed by Tregs (Nosbaum et al., 2016; Sojka and Fowell, 2011), did not rescue HFSC activation (Figure 5H). These findings suggest
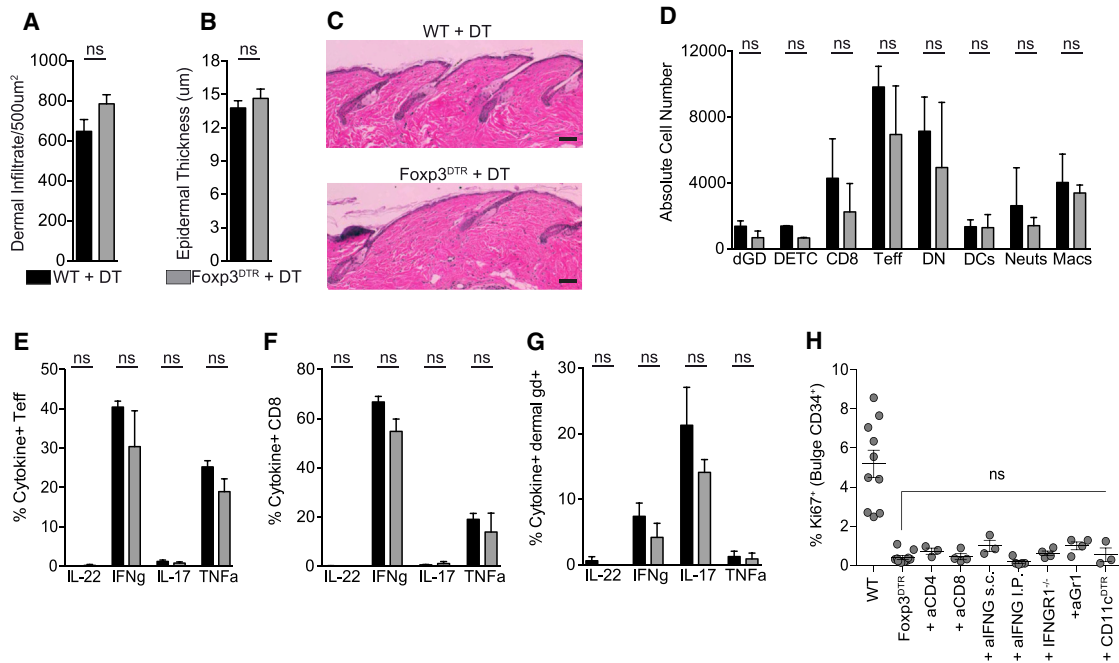
Figure 5. Transient Treg Loss Results in Minimal Skin Inflammation

(A and B) Control wild-type (WT) or Foxp3^DTR mice were depilated and treated with DT according to the "early" depletion protocol. (A) Total dermal infiltrate and (B) epidermal hyperplasia in DT-treated control (WT + DT) and Tregs-depleted (Foxp3^DTR + DT) dorsal skin on day 4 as measured by routine histology.

(C) Representative H&E staining of skin from WT and Foxp3^DTR mice on day 4.

(D) The absolute cell number of innate and adaptive immune cell subsets in skin as measured by flow cytometry. Single cell suspensions from day 1 skin were stimulated with PMA/ionomycin and the production of IL-22, IFNg, IL-17, and tumor necrosis factor alpha (TNF-α) was assessed by flow cytometry.

(E–G) The proportion of cytokine producing (E) CD4$^+$ Teff cells, (F) CD8$^+$ T cells, and (G) dermal $\gamma\delta^+$ T cells in dorsal skin.

(H) Flow cytometric quantification of Ki67$^+$ bulge HFSCs at day 4 post-depilation in immune cell-depleted and interferon-γ-neutralized (or interferon-γ signaling-deficient) mice.

Scale bars, 50 μm. Data are mean ± SEM. ns, no significant difference, unpaired Student's t test (A and B); two-way ANOVA (D–G); one-way ANOVA (H). Combined data from two experiments, with n = 3–4 mice per group.

See also Figure S5.

that suppression of inflammation is not a major mechanism by which Tregs promote HFSC function early in the process of hair regeneration.

Regulatory T Cells in Skin Preferentially Express the Notch Ligand Jag1

In an attempt to delineate potential mechanisms by which Tregs promote HFSC function, we compared the transcriptome of Tregs isolated from telogen skin with Tregs isolated from SDLNs (Table S2). We hypothesized that pathways involved in this process would be preferentially expressed in skin Tregs when compared to Tregs found in SDLNs. Consistent with heightened activation of Tregs in tissues (Burzyn et al., 2013; Feuerer et al., 2009; Sanchez Rodriguez et al., 2014), differential expression analyses revealed increased abundance of genes associated with Treg function in skin compared to SDLN Tregs, including CTLA-4, ICOS, and IL-10 (Figure 6A). Interestingly, Jag1, a ligand of the Notch signaling pathway, was among the highest differentially expressed genes between skin and SDLN Tregs (Figure 6A). Tregs in skin expressed ~150-fold more Jag1 transcript than SDLN Tregs (p value = 3.4 × 10^{-32}; Figure 6B). Assessment of Jag1 protein expression by flow cytometry confirmed greater

expression in skin Tregs relative to SDLN Tregs and increased expression on Tregs in telogen skin as compared to Tregs in anagen skin (Figures 6C and S6A–S6D). In addition, Treg-lineage expression of Jag1 was independently validated by qPCR, relative to CD4$^+$ Teff cells and CD8$^+$ T cells (Figure S6E). Aside from preferential expression on skin Tregs, Jag1 was an especially interesting candidate given the established role of the Notch pathway in HFSC biology (Blanpain et al., 2006; Estrach et al., 2006; Vauclair et al., 2005). Having identified skin Treg expression of Jag1, we next sought to determine if Notch target gene transcripts (Meier-Stiegen et al., 2010) were differentially expressed in HFSCs in the presence or absence of Tregs. Genome-wide RNA-seq analysis of HFSCs isolated 4 days after anagen induction in the presence or absence of Tregs revealed a differential signature of Notch target genes (Figures 6D and 6E). Of the 1,174 differentially expressed genes between the two groups, 84 genes (~7%) were known transcriptional targets of the Notch signaling pathway (p value of the overlap = 5.21 × 10^{-27}). Collectively, these results indicate that Tregs in murine skin preferentially express the Notch ligand, Jag1, and in the absence of Tregs, Notch signaling is significantly altered in HFSCs.
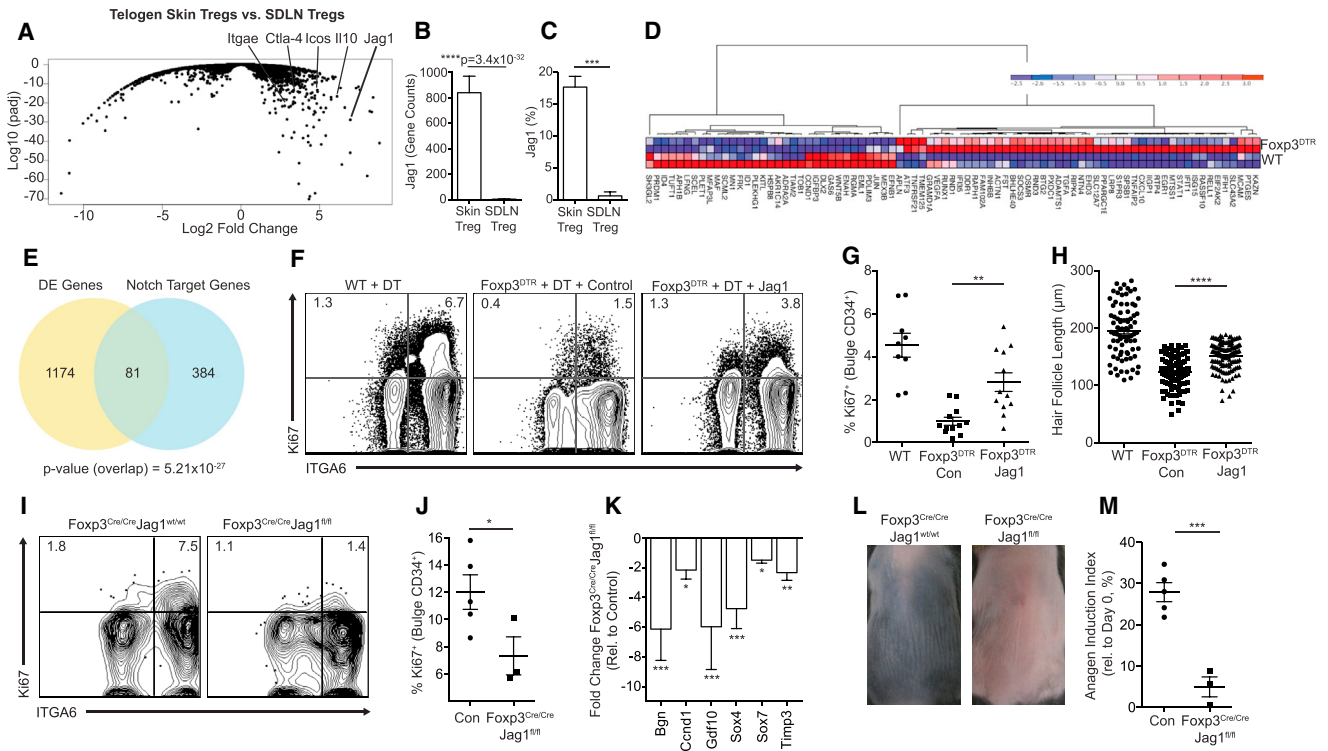
Figure 6. Treg Expression of Jagged 1 Is Required for Efficient HFSC Activation and Anagen Induction

RNA sequencing was performed on telogen skin Tregs and Tregs isolated from SDLNs.

(A) Volcano plot comparing expression profile of skin versus SDLN Tregs.

(B) Raw gene counts of Jagged 1 (Jag1) transcripts as quantified by RNA sequencing (n = 4 for skin Tregs and n = 3 for SDLN Tregs).

(C) Flow cytometric quantification of Jag1 expression on SDLN Tregs and skin Tregs (n = 4 for both skin and SDLN Tregs). RNA sequencing was performed on FACS purified bulge HFSCs at day 4 post-depilation from control (WT) or Treg-depleted (Foxp3^{DTR}) mice.

(D) Hierarchical clustering of differential expression of Notch target genes in HFSCs sequenced from control (WT) and Treg-depleted (DTR) mice, depicted as a heatmap.

(E) Venn diagram depicting the overlap between the total differentially expressed (DE) genes and known Notch target genes. P value represents the significance of the overlap as determined by a chi-square test.

(F) Jag1-Fc-coated or control Fc-coated beads were administered subcutaneously in Treg-depleted mice on days −2, −1, 1, and 3. All mice were depilated on day 0. Representative flow cytometric plots 4 days post-depilation gated on HFSCs from WT and Foxp3^{DTR} mice treated with control or Jag1-Fc-coated beads.

(G and H) Quantification of Ki67$^+$ bulge (G) HFSCs and (H) HF length 4 days post-depilation.

(I) Control (i.e., Foxp3Cre/CreJag1wt/wt) or Foxp3Cre/CreJag1fl/fl mice were depilated to induce anagen. Representative flow cytometric plots.

(J) Quantification of Ki67$^+$ bulge HFSCs.

(K) Fold change in HFSC differentiation genes as measured by qRT-PCR.

(L and M) Representative photos (L) and quantification (M) of skin pigmentation.

RNA-seq experiments were conducted using two to four biological samples (A, D, and E). Data are combined from three independent experiments (F–H). One representative experiment of two (I–M). Data are mean ± SEM. *p < 0.05, **p < 0.01 ***p < 0.001, ****p < 0.001, RNA-seq differential expression analysis, skin Tregs versus SDLN Tregs (B); unpaired t test (C, J, and M); one-way ANOVA (G, H, and K).

See also Figure S6 and Table 2.

Regulatory T Cell Expression of Jag1 Promotes HFSC Function

To functionally determine if Notch signaling plays a role in Treg-mediated enhancement of HFSC activation, we attempted to rescue the proliferative defect observed in HFSCs in Treg-depleted mice by the exogenous addition of Jag1 (Vas et al., 2004). Microbeads coated with Jag1-Fc or control Fc were subcutaneously administered to DT-treated Foxp3^{DTR} mice, and activation of HFSCs was quantified by flow cytometry 4 days post-depilation. In these experiments, exogenous Jag1 was able to partially rescue HFSC activation and induction of anagen in the absence of Tregs (Figures 6F–6H). To definitively test whether Jag1 expression on Tregs plays a role in HFSC differentiation and anagen induction, mice expressing a Jag1 conditional allele (Brooker et al., 2006) (Jag1$^{fl/fl}$) were crossed to Foxp3-cre mice (Rubtsov et al., 2008) to specifically ablate Jag1 expression in Tregs. Foxp3$^{Cre/Cre}$Jag1$^{fl/fl}$ mice in telogen phase of the HF cycle were depilated and HFSC proliferation, differentiation and kinetics of anagen induction were quantified. Early after depilation, Foxp3$^{Cre/Cre}$Jag1$^{fl/fl}$ mice had significantly attenuated proliferative capacity of integrin-α6^{high} CD34$^+$ bulge HFSCs when compared to age- and gender- matched littermate controls

(Figures 6I and 6J). Absolute cell numbers of HFSCs in Foxp3^{Cre-}Jag1$^{fl/fl}$ mice and the ratio of Treg-to-HFSCs both in the steady-state and post-depilation were unchanged relative to Foxp3^{Cre}/Jag1$^{wt/wt}$ mice (Figures S6F–S6H), suggesting that Jag1 loss in Tregs does not alter the overall composition of Tregs and/or HFSCs in skin.

In addition, relative to control mice, deletion of Jag1 in Tregs resulted in a significant reduction in the expression of key epidermal differentiation genes, including Bgn, Ccnd1, Gdf10, Sox4, Sox7, and Timp3 (Figure 6K). Given the early requirement for Tregs in HFSC activation, we assayed the kinetics of anagen induction by quantifying dorsal skin pigmentation (the earliest clinical marker of initiation of this process) (Müller-Röver et al., 2001). Consistent with the diminished proliferative and differentiation capacity of HFSCs, anagen entry in Foxp3$^{Cre/Cre}$Jag1$^{fl/fl}$ dorsal skin was significantly attenuated relative to control dorsal skin (Figures 6L and 6M), revealing a role for Jag1 expression on Tregs in facilitating anagen induction. Taken together, our results suggest that the Jag1-Notch pathway plays a role in the ability of skin Tregs to promote HFSC function.

DISCUSSION

There is an emerging body of literature suggesting that Tregs represent a highly complex and heterogeneous lymphocyte lineage that possess specialized functions in the tissues in which they reside (Panduro et al., 2016). Here, we describe a previously unrecognized role of skin-resident Tregs in promoting epithelial SC function. We demonstrate a critical requirement for Tregs in HF regeneration through facilitation of epithelial SC proliferation and differentiation. Consistent with studies examining Tregs in muscle and lung (Arpaia et al., 2015; Burzyn et al., 2013; Villalta et al., 2014), we establish a role for Tregs in mediating a vital regenerative function of skin. The fact that skin Tregs facilitate HF regeneration by promoting HFSC activation is consistent with the observation that Tregs in bone marrow co-localize with hematopoietic SCs and support their function in this tissue (Fujisaki et al., 2011). Collectively, these findings suggest that a fundamental property of both intra- and extra-lymphoid Tregs is to influence SC biology and supports the view that a functional relationship between Tregs and SCs is a generalizable concept intrinsic to many tissues.

The finding that short-term depletion of Tregs did not alter accumulation or activation of the major immune cell subsets in skin suggests that transient Treg loss does not result in overt skin inflammation. Consistent with this observation, co-depletion of inflammatory cells (and a major inflammatory pathway) with Tregs did not restore HFSC function. Taken together, these results suggest that suppression of inflammation is not the major mechanism by which Tregs promote HFSC proliferation and differentiation. Furthermore, Treg lineage-specific deletion of Jag1 largely resembled loss of the entire Treg population, with respect to HFSC proliferation, differentiation, and the capacity to induce HF entry into anagen. While our data do not definitively rule out the potential for Tregs to exert their effects on epithelial SCs by suppressing immune activation, they suggest that Tregs in skin have the ability to modulate the biology of tissue SCs independently of this function. Whether this is mediated by a subset of

Tregs or the bulk skin-resident Treg population and whether expression of Jag1 is the only mechanism that Tregs utilize in this process remain to be determined.

A classic function of HFSCs is to drive HF cycling and HF regeneration (Blanpain and Fuchs, 2009; Morris et al., 2004; Trempus et al., 2003). However, an alternative function of these cells is to aid in epidermal barrier repair after injury (Ito et al., 2005). Unlike HF cycling, epidermal barrier repair is associated with marked tissue inflammation. Thus, in addition to their role in promoting HF cycling, it is interesting to speculate that skin Tregs also play a role in facilitating the function of HFSCs in the context of epidermal barrier repair. In this capacity, Tregs may regulate both inflammatory and non-inflammatory pathways to mediate their effects. It is currently unknown whether Tregs in skin influence HFSC biology in contexts other than HF cycling.

Our results highlight the Notch pathway as a mechanism employed by skin-resident Tregs to facilitate HFSC function during HF cycling. Skin Tregs in proximity to the HF are activated, by currently unknown mechanisms, as the follicle transitions from telogen to anagen. These activated Tregs produce the Notch ligand, Jag1, which stimulates the proliferation and differentiation of HFSCs and drives progression through the anagen phase. The ability of one immune cell population in skin to regulate the behavior of SCs in that tissue raises the novel possibility that immune control of stem cell function may be a general paradigm applicable to stem cells in other tissues. It will be important to determine whether this principle extends to human diseases of epithelial dysfunction and whether Tregs can be exploited to develop new therapies for SC-mediated tissue regenerative disorders.

STAR★METHODS

Detailed methods are provided in the online version of this paper and include the following:

- KEY RESOURCES TABLE
- CONTACT FOR REAGENT AND RESOURCE SHARING
- EXPERIMENTAL MODELS AND SUBJECT DETAILS
  - Experimental Animals
- METHOD DETAILS
  - Anagen induction
  - In vivo T$_{reg}$ cell depletion
  - Immune cell co-depletions
  - Treg Conditional Jag1 Deletion
  - Tissue processing
  - Histology
  - In vivo Jag1 rescue
  - RNA-Sequencing analysis and Quantitative PCR
  - Intravital 2-photon imaging of T$_{regs}$ in dorsal skin
  - Statistical analyses
  - Data and Software Availability

SUPPLEMENTAL INFORMATION

Supplemental Information includes six figures, two tables, and two movies and can be found with this article online at http://dx.doi.org/10.1016/j.cell.2017.05.002.

REFERENCES

Anders, S., and Huber, W. (2010). Differential expression analysis for sequence count data. Genome Biol. 11, R106.

Anders, S., Pyl, P.T., and Huber, W. (2015). HTSeq–a Python framework to work with high-throughput sequencing data. Bioinformatics 31, 166–169.

Arpaia, N., Green, J.A., Moltedo, B., Arvey, A., Hemmers, S., Yuan, S., Treuting, P.M., and Rudensky, A.Y. (2015). A distinct function of regulatory T cells in tissue protection. Cell 162, 1078–1089.

Blanpain, C., and Fuchs, E. (2009). Epidermal homeostasis: a balancing act of stem cells in the skin. Nat. Rev. Mol. Cell Biol. 10, 207–217.

Blanpain, C., Lowry, W.E., Pasolli, H.A., and Fuchs, E. (2006). Canonical notch signaling functions as a commitment switch in the epidermal lineage. Genes Dev. 20, 3022–3035.

Boldajipour, B., Nelson, A., and Krummel, M.F. (2016). Tumor-infiltrating lymphocytes are dynamically desensitized to antigen but are maintained by homeostatic cytokine. JCI Insight 1, e89289.

Brooker, R., Hozumi, K., and Lewis, J. (2006). Notch ligands with contrasting functions: Jagged1 and Delta1 in the mouse inner ear. Development 133, 1277–1286.

Broz, M.L., Binnewies, M., Boldajipour, B., Nelson, A.E., Pollack, J.L., Erle, D.J., Barczak, A., Rosenblum, M.D., Daud, A., Barber, D.L., et al. (2014). Dissecting the tumor myeloid compartment reveals rare activating antigen-presenting cells critical for T cell immunity. Cancer Cell 26, 638–652.

Burzyn, D., Kuswanto, W., Kolodin, D., Shadrach, J.L., Cerletti, M., Jang, Y., Sefik, E., Tan, T.G., Wagers, A.J., Benoist, C., and Mathis, D. (2013). A special population of regulatory T cells potentiates muscle repair. Cell 155, 1282–1295.

Castela, E., Le Duff, F., Butori, C., Ticchioni, M., Hofman, P., Bahadoran, P., Lacour, J.-P., and Passeron, T. (2014). Effects of low-dose recombinant interleukin 2 to promote T-regulatory cells in alopecia areata. JAMA Dermatol. 150, 748–751.

Chen, T., Heller, E., Beronja, S., Oshimori, N., Stokes, N., and Fuchs, E. (2012). An RNA interference screen uncovers a new molecule in stem cell self-renewal and long-term regeneration. Nature 485, 104–108.

Chow, Z., Mueller, S.N., Deane, J.A., and Hickey, M.J. (2013). Dermal regulatory T cells display distinct migratory behavior that is modulated during adaptive and innate inflammation. J. Immunol. 191, 3049–3056.

Cipolletta, D., Feuerer, M., Li, A., Kamei, N., Lee, J., Shoelson, S.E., Benoist, C., and Mathis, D. (2012). PPAR-γ is a major driver of the accumulation and phenotype of adipose tissue Treg cells. Nature 486, 549–553.

Clark, R.A., Chong, B., Mirchandani, N., Brinster, N.K., Yamanaka, K., Dowgiert, R.K., and Kupper, T.S. (2006). The vast majority of CLA+ T cells are resident in normal skin. J. Immunol. 176, 4431–4439.

Cotsarelis, G., Sun, T.T., and Lavker, R.M. (1990). Label-retaining cells reside in the bulge area of pilosebaceous unit: implications for follicular stem cells, hair cycle, and skin carcinogenesis. Cell 61, 1329–1337.

de Hoon, M.J.L., Imoto, S., Nolan, J., and Miyano, S. (2004). Open source clustering software. Bioinformatics 20, 1453–1454.

Estrach, S., Ambler, C.A., Lo Celso, C., Hozumi, K., and Watt, F.M. (2006). Jagged 1 is a beta-catenin target gene required for ectopic hair follicle formation in adult epidermis. Development 133, 4427–4438.

Feuerer, M., Herrero, L., Cipolletta, D., Naaz, A., Wong, J., Nayer, A., Lee, J., Goldfine, A.B., Benoist, C., Shoelson, S., and Mathis, D. (2009). Lean, but not obese, fat is enriched for a unique population of regulatory T cells that affect metabolic parameters. Nat. Med. 15, 930–939.

Friedman, R.S., Beemiller, P., Sorensen, C.M., Jacobelli, J., and Krummel, M.F. (2010). Real-time analysis of T cell receptors in naive cells in vitro and in vivo reveals flexibility in synapse and signaling dynamics. J. Exp. Med. 207, 2733–2749.

Fujisaki, J., Wu, J., Carlson, A.L., Silberstein, L., Putheti, P., Larocca, R., Gao, W., Saito, T.I., Lo Celso, C., Tsuyuzaki, H., et al. (2011). In vivo imaging of Treg cells providing immune privilege to the haematopoietic stem-cell niche. Nature 474, 216–219.

Gratz, I.K., Truong, H.-A., Yang, S.H.-Y., Maurano, M.M., Lee, K., Abbas, A.K., and Rosenblum, M.D. (2013). Cutting Edge: memory regulatory t cells require IL-7 and not IL-2 for their maintenance in peripheral tissues. J. Immunol. 190, 4483–4487.

Headley, M.B., Bins, A., Nip, A., Roberts, E.W., Looney, M.R., Gerard, A., and Krummel, M.F. (2016). Visualization of immediate immune responses to pioneer metastatic cells in the lung. Nature 531, 513–517.

Ito, M., Liu, Y., Yang, Z., Nguyen, J., Liang, F., Morris, R.J., and Cotsarelis, G. (2005). Stem cells in the hair follicle bulge contribute to wound repair but not to homeostasis of the epidermis. Nat. Med. 11, 1351–1354.

Jaks, V., Barker, N., Kasper, M., van Es, J.H., Snippert, H.J., Clevers, H., and Toftgård, R. (2008). Lgr5 marks cycling, yet long-lived, hair follicle stem cells. Nat. Genet. 40, 1291–1299.

Kim, J.M., Rasmussen, J.P., and Rudensky, A.Y. (2007). Regulatory T cells prevent catastrophic autoimmunity throughout the lifespan of mice. Nat. Immunol. 8, 191–197.

Lecuit, T., and Lenne, P.-F. (2007). Cell surface mechanics and the control of cell shape, tissue patterns and morphogenesis. Nat. Rev. Mol. Cell Biol. 8, 633–644.

Levy, V., Lindon, C., Harfe, B.D., and Morgan, B.A. (2005). Distinct stem cell populations regenerate the follicle and interfollicular epidermis. Dev. Cell 9, 855–861.

Li, H., Handsaker, B., Wysoker, A., Fennell, T., Ruan, J., Homer, N., Marth, G., Abecasis, G., and Durbin, R.; 1000 Genome Project Data Processing Subgroup (2009). The Sequence Alignment/Map format and SAMtools. Bioinformatics 25, 2078–2079.

Lin, W., Haribhai, D., Relland, L.M., Truong, N., Carlson, M.R., Williams, C.B., and Chatila, T.A. (2007). Regulatory T cell development in the absence of functional Foxp3. Nat. Immunol. 8, 359–368.

Lindsay, R.S., Corbin, K., Mahne, A., Levitt, B.E., Gebert, M.J., Wigton, E.J., Bradley, B.J., Haskins, K., Jacobelli, J., Tang, Q., et al. (2015). Antigen recognition in the islets changes with progression of autoimmune islet infiltration. J. Immunol. *194*, 522–530.

Looney, M.R., Thornton, E.E., Sen, D., Lamm, W.J., Glenny, R.W., and Krummel, M.F. (2011). Stabilized imaging of immune surveillance in the mouse lung. Nat. Methods *8*, 91–96.

Lowry, W.E., Blanpain, C., Nowak, J.A., Guasch, G., Lewis, L., and Fuchs, E. (2005). Defining the impact of beta-catenin/Tcf transactivation on epithelial stem cells. Genes Dev. *19*, 1596–1611.

Matheu, M.P., Teijaro, J.R., Walsh, K.B., Greenberg, M.L., Marsolais, D., Parker, I., Rosen, H., Oldstone, M.B.A., and Cahalan, M.D. (2013). Three phases of CD8 T cell response in the lung following H1N1 influenza infection and sphingosine 1 phosphate agonist therapy. PLoS ONE *8*, e58033.

Meier-Stiegen, F., Schwanbeck, R., Bernoth, K., Martini, S., Hieronymus, T., Ruau, D., Zenke, M., and Just, U. (2010). Activated Notch1 target genes during embryonic cell differentiation depend on the cellular context and include lineage determinants and inhibitors. PLoS ONE *5*, e11481.

Morris, R.J., Liu, Y., Marles, L., Yang, Z., Trempus, C., Li, S., Lin, J.S., Sawicki, J.A., and Cotsarelis, G. (2004). Capturing and profiling adult hair follicle stem cells. Nat. Biotechnol. *22*, 411–417.

Müller-Röver, S., Handjiski, B., van der Veen, C., Eichmüller, S., Foitzik, K., McKay, I.A., Stenn, K.S., and Paus, R. (2001). A comprehensive guide for the accurate classification of murine hair follicles in distinct hair cycle stages. J. Invest. Dermatol. *117*, 3–15.

Nagao, K., Kobayashi, T., Moro, K., Ohyama, M., Adachi, T., Kitashima, D.Y., Ueha, S., Horiuchi, K., Tanizaki, H., Kabashima, K., et al. (2012). Stress-induced production of chemokines by hair follicles regulates the trafficking of dendritic cells in skin. Nat. Immunol. *13*, 744–752.

Nosbaum, A., Prevel, N., Truong, H.-A., Mehta, P., Ettinger, M., Scharschmidt, T.C., Ali, N.H., Pauli, M.L., Abbas, A.K., and Rosenblum, M.D. (2016). Cutting edge: regulatory T cells facilitate cutaneous wound healing. J. Immunol. *196*, 2010–2014.

Panduro, M., Benoist, C., and Mathis, D. (2016). Tissue Tregs. Annu. Rev. Immunol. *34*, 609–633.

Petukhova, L., Duvic, M., Hordinsky, M., Norris, D., Price, V., Shimomura, Y., Kim, H., Singh, P., Lee, A., Chen, W.V., et al. (2010). Genome-wide association study in alopecia areata implicates both innate and adaptive immunity. Nature *466*, 113–117.

Reich, M., Liefeld, T., Gould, J., Lerner, J., Tamayo, P., and Mesirov, J.P. (2006). GenePattern 2.0. Nat. Genet. *38*, 500–501.

Rubtsov, Y.P., Rasmussen, J.P., Chi, E.Y., Fontenot, J., Castelli, L., Ye, X., Treuting, P., Siewe, L., Roers, A., Henderson, W.R., Jr., et al. (2008). Regulatory T cell-derived interleukin-10 limits inflammation at environmental interfaces. Immunity *28*, 546–558.

Sanchez Rodriguez, R., Pauli, M.L., Neuhaus, I.M., Yu, S.S., Arron, S.T., Harris, H.W., Yang, S.H.-Y., Anthony, B.A., Sverdrup, F.M., Krow-Lucal, E., et al. (2014). Memory regulatory T cells reside in human skin. J. Clin. Invest. *124*, 1027–1036.

Sano, T., Kobayashi, T., Negoro, H., Sengiku, A., Hiratsuka, T., Kamioka, Y., Liou, L.S., Ogawa, O., and Matsuda, M. (2016). Intravital imaging of mouse urothelium reveals activation of extracellular signal-regulated kinase by stretch-induced intravesical release of ATP. Physiol. Rep. *4*, e13033.

Scharschmidt, T.C., Vasquez, K.S., Truong, H.-A., Gearty, S.V., Pauli, M.L., Nosbaum, A., Gratz, I.K., Otto, M., Moon, J.J., Liese, J., et al. (2015). A wave of regulatory T cells into neonatal skin mediates tolerance to commensal microbes. Immunity *43*, 1011–1021.

Sojka, D.K., and Fowell, D.J. (2011). Regulatory T cells inhibit acute IFN-γ synthesis without blocking T-helper cell type 1 (Th1) differentiation via a compartmentalized requirement for IL-10. Proc. Natl. Acad. Sci. USA *108*, 18336–18341.

Thornton, E.E., Looney, M.R., Bose, O., Sen, D., Sheppard, D., Locksley, R., Huang, X., and Krummel, M.F. (2012). Spatiotemporally separated antigen uptake by alveolar dendritic cells and airway presentation to T cells in the lung. J. Exp. Med. *209*, 1183–1199.

Trapnell, C., Pachter, L., and Salzberg, S.L. (2009). TopHat: discovering splice junctions with RNA-seq. Bioinformatics *25*, 1105–1111.

Trempus, C.S., Morris, R.J., Bortner, C.D., Cotsarelis, G., Faircloth, R.S., Reece, J.M., and Tennant, R.W. (2003). Enrichment for living murine keratinocytes from the hair follicle bulge with the cell surface marker CD34. J. Invest. Dermatol. *120*, 501–511.

Tumbar, T., Guasch, G., Greco, V., Blanpain, C., Lowry, W.E., Rendl, M., and Fuchs, E. (2004). Defining the epithelial stem cell niche in skin. Science *303*, 359–363.

Vas, V., Szilágyi, L., Pálóczi, K., and Uher, F. (2004). Soluble Jagged-1 is able to inhibit the function of its multivalent form to induce hematopoietic stem cell self-renewal in a surrogate in vitro assay. J. Leukoc. Biol. *75*, 714–720.

Vauclair, S., Nicolas, M., Barrandon, Y., and Radtke, F. (2005). Notch1 is essential for postnatal hair follicle development and homeostasis. Dev. Biol. *284*, 184–193.

Villalta, S.A., Rosenthal, W., Martinez, L., Kaur, A., Sparwasser, T., Tidball, J.G., Margeta, M., Spencer, M.J., and Bluestone, J.A. (2014). Regulatory T cells suppress muscle inflammation and injury in muscular dystrophy. Sci. Transl. Med. *6*, 258ra142.

Vinegoni, C., Lee, S., Gorbatov, R., and Weissleder, R. (2012). Motion compensation using a suctioning stabilizer for intravital microscopy. Intravital *1*, 115–121.

Zaid, A., Mackay, L.K., Rahimpour, A., Braun, A., Veldhoen, M., Carbone, F.R., Manton, J.H., Heath, W.R., and Mueller, S.N. (2014). Persistence of skin-resident memory T cells within an epidermal niche. Proc. Natl. Acad. Sci. USA *111*, 5307–5312.

STAR★METHODS

KEY RESOURCES TABLE

REAGENT or RESOURCE	SOURCE	IDENTIFIER
Antibodies		
Anti-Mouse/Rat Foxp3 eFluor 450	eBioscience	Cat# 48-5773-82
Anti-Human Ki67 PE-Cy7	BD	Cat# 561283
Anti-Mouse CD25 APC-eFluor 780	eBioscience	Cat# 47-0251-82
Anti-Mouse/Rat CD278 (ICOS) FITC	eBioscience	Cat# 11-9949-80
Anti-Mouse CD357 (GITR) APC	eBioscience	Cat# 17-5874-81
Anti-Mouse CD152 (CTLA4) PE	BD	Cat# 553720
Rabbit anti-GFP	Invitrogen	Cat# A11122
Chicken anti-Keratin-15	Biolegend	Cat# Poly19339
Anti-mouse/human ITGA6	BD	Cat# 555734
Purified Ki67	Dako	Cat# GA626
Anti-Mouse CD45 Alexa Fluor 700	eBioscience	Cat# 56-0451-82
Brilliant Violet 605 anti-mouse Ly-6A/E (Sca-1) Antibody	Biolegend	Cat# 108133
Anti-Mouse CD34 Alexa Fluor 647	BD	Cat# 560233
Anti-Mouse CD326 (EpCAM) APC-eFluor 780	eBioscience	Cat# 47-5791-82
Anti-Human/Mouse CD49f (Integrin a 6) FITC	eBioscience	Cat# 11-0495-82
Anti-Mouse TCR gd PerCP-Cy 5.5	Biolegend	Cat# 118117
Brilliant Violet 605 anti-mouse CD8a Antibody	Biolegend	Cat# 100743
Brilliant Violet 711 anti-mouse CD3 Antibody	Biolegend	Cat# 100241
Brilliant Violet 650 anti-mouse CD4 Antibody	Biolegend	Cat# 100545
Brilliant Violet 711 anti-mouse/human CD11b Antibody	Biolegend	Cat# 101241
Brilliant Violet 650 anti-mouse CD11c Antibody	Biolegend	Cat# 117339
Anti-Mouse Ly-6G PE-Cy7	BD	Cat# 560601
Brilliant Violet 785 anti-mouse F4/80 Antibody	Biolegend	Cat# 123141
Brilliant Violet 605 anti-mouse Ly-6C Antibody	Biolegend	Cat# 128035
Purified Rat Anti-Mouse CD16/CD32	BD	Cat# 553141
Anti-Mouse IL-22 PerCP-eFluor 710	eBioscience	Cat# 46-7221-80
Brilliant Violet 650 anti-mouse IFN-γ Antibody	Biolegend	Cat# 505831
Anti-Mouse/Rat IL-17A PE-Cyanine7	eBioscience	Cat# 25-7177-80
Anti-Mouse TNFa PE	eBioscience	Cat# 12-7321-82
Anti-Mouse CD339 (Jagged 1) PE	eBioscience	Cat# 12-3391-80
Armenian Hamster IgG Isotype Control PE	eBioscience	Cat# 12-4888-81
Anti-Mouse MHC Class II (I-A/I-E) eFluor 450	eBioscience	Cat# 48-5321-80
InVivoMAb anti-mouse CD4	BioXcell	Cat#: BE0289
InVivoMAb anti-mouse CD8α	BioXcell	Cat#: BE0061
InVivoMAb anti-mouse IFNγ	BioXcell	Cat#: BE0055
InVivoMAb anti-mouse Ly6G/Ly6C (Gr-1)	BioXcell	Cat#: BE0075
Chemicals, Peptides, and Recombinant Proteins		
Collagenase from *Clostridium* histolyticum, Type XI	Sigma-Aldrich	Cat#C9407
DNase	Sigma-Aldrich	Cat#DN25
Hyaluronidase from bovine testes	Sigma-Aldrich	Cat#H3506
Tween™ 80	Fisher	Cat#T164-500
Recombinant Human IgG1 Fc, CF	R&D	Cat# 110-HG-00
Recombinant Rat Jagged 1 Fc Chimera Protein, CF	R&D	Cat# 599-JG-100

Continued

REAGENT or RESOURCE	SOURCE	IDENTIFIER
Affi-Gel Blue Gel	Bio-Rad	Cat# 1537301
Evans Blue	Sigma-Aldrich	Cat# E2129
Cell Stimulation Cocktail (500X)	Tonbo	Cat# TNB-4975
Nair Men Hair Removal Body Cream	Nair	Walgreens, San Francisco, CA
Diphtheria Toxin from Corynebacterium diphtheriae	Sigma-Aldrich	D0564
Critical Commercial Assays		
Click-iT® Plus EdU Alexa Fluor 488 Flow Cytometry Assay Kit	ThermoFisher	Cat# C10632
PureLink® RNA Mini Kit	ThermoFisher	Cat# 12183018A
iScript Kit Advanced cDNA Synthesis Kit for RT-qPCR	Bio-Rad	Cat#1725038
Mouse FoxP3 Buffer Set	eBiosciences	Cat#00-5523-00
Ghost Dye™ Violet 510 Live/Dead Stain	Tonbo Biosciences	Cat#13-0870-T100
0.5% Trypsin-EDTA (10x), no phenol red	ThermoFisher	Cat# 1540054
Bgn	ThermoFisher	Cat# Mm01191753_m1
Ccnd1	ThermoFisher	Cat# Mm00432359_m1
Gdf10	ThermoFisher	Cat# Mm01220860_m1
Sox4	ThermoFisher	Cat# Mm00486320_s1
Sox7	ThermoFisher	Cat# Mm00776876_m1
Timp3	ThermoFisher	Cat# Mm00441826_m1
TaqMan Gene Expression Master Mix	ThermoFisher	Cat# 4369510
Deposited Data		
Raw Data files for RNA-Sequencing - Tregs	NCBI Gene Expression Omnibus	GEO: GSE76138
Raw Data files for RNA-Sequencing - HFSCs	NCBI Gene Expression Omnibus	GEO: GSE76102
Experimental Models: Organisms/Strains		
Mouse: B6.129(Cg)-Foxp3$^{tm3(DTR/GFP)Ayr}$/J (Foxp3DTR)	The Jackson Laboratory	016958
Mouse: B6.Cg-Foxp3^{tm2Tch}/J (Foxp3GFP)	The Jackson Laboratory	006772
Mouse: B6.129(Cg)-Foxp3$^{tm4(YFP/icre)Ayr}$/J (Foxp3Cre/Cre)	The Jackson Laboratory	016959
Mouse: B6;129S-Jag1^{tm2Grid}/J (Jag1fl/fl)	The Jackson Laboratory	010618
Mouse: B6.129S7-Ifngr1^{tm1Agt}/J (IFNGR1−/−)	The Jackson Laboratory	003288
Mouse: B6.FVB-Tg(Itgax-DTR/EGFP)57Lan/J (CD11cGFP-DTR)	The Jackson Laboratory	004509
Mouse: C57BL/6J wild type (WT)	The Jackson Laboratory	000664
Mouse: B6.129S6-Rag2^{tm1Fwa} N12 (Rag2−/−)	Taconic	RAGN12
Software and Algorithms		
TopHat	(Trapnell et al., 2009)	https://ccb.jhu.edu/software/tophat/index.shtml
SAMtools	(Li et al., 2009)	http://www.htslib.org
DESeq2	(Anders and Huber, 2010)	https://bioconductor.org/packages/release/bioc/html/DESeq2.html
HTSeq	(Anders et al., 2015)	http://www-huber.embl.de/users/anders/HTSeq/doc/overview.html
R Statistical Computing Software	The R Foundation https://www.r-project.org/	https://www.r-project.org/
GraphPad Prism	GraphPad Software, Inc	http://www.graphpad.com/scientific-software/prism/
FlowJo	FlowJo, LLC	https://www.flowjo.com/solutions/flowjo
Imaris	Bitplane	Version 8.4
ImageJ	MIH	Version 1.50i

CONTACT FOR REAGENT AND RESOURCE SHARING

Further information and requests for resources and reagents should be directed to and will be fulfilled by the Lead Contact, Michael Rosenblum (Michael.Rosenblum@ucsf.edu).

EXPERIMENTAL MODELS AND SUBJECT DETAILS

Experimental Animals

Mice were bred and/or maintained in the UCSF specific pathogen-free facility in accordance with the guidelines of the Laboratory Animal Resource Center and Institutional Animal Care and Use Committee of the University of California San Francisco (UCSF). All mice used in experiments were socially houses under a 12 hr light/dark cycle. All experiments were initiated in the telogen phase of the HF cycle in 7-10 week old mice, unless otherwise specified.

METHOD DETAILS

Anagen induction

Dorsal hair was first shortened with clippers before applying depilatory cream (Nair) to the shaved region for a period of exactly 30 s before wiping clean. For monitoring of clinical hair regrowth, standardized pictures were taken with a ruler on the day of depilation (day 0) and then at the indicated time points until day 14. Anagen induction was quantified using intensity analysis on ImageJ software (v1.46r, NIH, USA) at each time point or as a percent of pigmented dorsal skin relative to baseline (day 0). All experiments conducted in $Foxp3^{Cre/Cre}Jag1^{fl/fl}$ or control mice (i.e., $Foxp3^{Cre/Cre}Jag1^{wt/wt}$ or $Foxp3^{wt/wt}Jag1^{fl/fl}$) were harvested on day 10 post depilation. For monitoring of the synchronous HF cycle, dorsal hair was clipped and pictures taken at the indicated time points for quantification. For flow cytometric analysis and cell sorting for RNA-sequencing experiments, epidermal cells were prepared from mice harvested at day 4 post-depilation.

In vivo T_{reg} cell depletion

The optimal dose of each DT Lot (Sigma) was initially determined by assessing the efficiency of skin T_{reg} depletion by flow cytometry. Accordingly, $Foxp3^{DTR}$ and control mice were injected i.p. with DT at 15 ng/g or 30ng/g body weight, according to three regimens: mice were injected with DT on day −2 and day −1 prior to depilation (performed on day 0) and then every other day until day 4 (early; 4 doses total) or day 14 (constitutive; 10 doses total). For late T_{reg} depletion studies, DT was administered first on day 7 and then every other day until day 14 (4 doses total). For Treg depletion during the natural HF cycle in $Foxp3^{DTR}$ mice, DT or PBS was injected at postnatal day 21 (P21), P22, and P24.

Immune cell co-depletions

All antibodies for depletion studies were purchased from BioXcell (West Lebanon, NH, USA). Anti-CD4 (GK1.5, 400 μg per injection), anti-CD8 (2.43, 400 μg per injection), anti-interferon gamma (IFNG, XMG1.2, 500 μg per injection), anti-Gr1 (RB6-8C5, 100 μg per injection) were administered i.p with DT according to the early T_{reg} cell ablation regimen in $Foxp3^{DTR}$ mice. For subcutaneous anti-IFNG administration, 100 μg was injected directly into dorsal skin on the day of depilation (day 0) and then on day 1 and day 3. For $IFNGR1^{-/-}$ hosts, anti-CD4 was administered on days −2, −1, day 1 and day 3 to deplete $CD4^{+}$ T cells. For $CD11c^{DTR/GFP}$ hosts, 15ng/g DT and anti-CD4 was administered on days −2, −1, day 1 and day 3 to deplete CD11c-expressing myeloid cells and $CD4^{+}$ T cells, respectively.

Treg Conditional Jag1 Deletion

All experimental mice were generated from breeders that consisted of Foxp3-Cre homozygous/Jag1 heterozygous females ($Foxp3^{Cre/Cre}Jag1^{wt/fl}$) crossed to Foxp3-Cre hemizygous/Jag1 heterozygous males ($Foxp3^{Cre}Jag1^{wt/fl}$). Genotyping of the resulting offspring determined that all female mice were homozygous for Foxp3-Cre and all males hemizygous for Foxp3-Cre. For the floxed Jag1 allele mice were either wild-type ($Jag1^{wt/wt}$), heterozygous ($Jag1^{wt/fl}$), or homozygous ($Jag1^{fl/fl}$). Unless otherwise stated, only age, gender, and littermate matched Foxp3-Cre homozygous (or hemizygous for males)/Jag1-wild-type mice were used as controls ($Foxp3^{Cre/Cre}Jag1^{wt/wt}$) and Foxp3-Cre homozygous (or hemizygous for males) Jag1 flox-homozygous mice for the experimental group ($Foxp3^{Cre/Cre}Jag1^{fl/fl}$).

Tissue processing

Preparation of single cell suspensions from SDLNs or full thickness skin excised at indicated time points during the synchronous HF cycle for T_{reg} analysis or cell sorting by flow cytometry was performed as previously described (Scharschmidt et al., 2015). Briefly, Isolation of cells from axillary, brachial and inguinal lymph nodes (referred to as skin draining lymph nodes, SDLNs) for flow cytometry was performed by mashing tissue over 100 μm sterile filters For isolation of dorsal skin cells, mouse dorsal skin was harvested and lightly defatted. It was then minced finely with scissors and re-suspended in a 50ml conical with 3 mL of digestion mix (composed of 2mg/ml collagenase XI, 0.5mg/ml hyaluronidase and 0.1mg/ml DNase in RPMI with 1% HEPES, 1% penicillin-streptomycin and

10% fetal calf serum), followed by incubation in a shaking incubator at 37°C at 250 rpm for 50 min. An additional 20 mL of RPMI/HEPES/P-S/FCS media was then added and the 50ml conical was shaken by hand for 30-45 s. Another 20 mL of media was added and the suspension filtered through a sterile 100 μm cell strainer followed by a 40el cell strainer into a new 50ml conical. The suspension was then pelleted and re-suspended in PBS for cell counting and staining. Epithelial cell preparations from depilated mice were prepared for flow cytometric analysis or HFSC sorting as previously described (Nagao et al., 2012). Briefly, mouse dorsal skin was harvested and lightly defatted before placing upon 2 mL of Trypsin-EDTA (0.5%, 10x, ThermoFisher), followed by incubation at 37°C for 1 hr. Epidermal cells were then scraped off into a petri dish containing RPMI/HEPES/P-S/FCS media and the cell suspension then filtered through a sterile 100 μm cell strainer followed by a 40el cell strainer into a new 50ml conical. The suspension was then pelleted and re-suspended in PBS for cell counting and staining. Following isolation from the tissue, cells were labeled stained in PBS for 30 min at 4°C with surface antibodies and a live dead marker (Ghost Dye™ Violet 510, Tonbo Biosciences). For intracellular staining, cells were fixed and permeabilized using reagents and protocol from the Foxp3 staining buffer kit (eBioscience). Fluorophore-conjugated antibodies specific for mouse cell surface antigens and intracellular transcription factors were purchased from eBioscience, BD Biosciences or Biolegend as detailed in the Key Resources Table. Samples were run on a Fortessa (BD Biosciences) in the UCSF Flow Cytometry Core. Treg cells from skin and SDLNs were sorted on a FACS Aria2 (BD Biosciences). For all experiments, voltages were standardized using SPHERO Rainbow calibration particles (BD Biosciences). An automated cell counter (NucleoCounter® NC-200, Chemometec) was used to enumerate cell numbers from single cell suspensions and for calculations of absolute cell numbers. Flow cytometry data was analyzed using FlowJo software (FlowJo, LLC). Strict dead cell and doublet cell exclusion criteria were included for all immune cell analysis, followed by pre-gating for all hematopoietic cells as CD45$^+$. Lymphoid cells were gated as $\gamma\delta$-TCR$^-$CD3$^-$ double negative cells (DN), $\gamma\delta$-TCR$^+$CD3$^+$ dermal $\gamma\delta$ T cells (dGD), $\gamma\delta$-TCR^{hi}CD3^{hi} dendritic epidermal T cells (DETCs), CD3$^+$CD8$^+$ T cells (CD8), CD3$^+$CD4$^+$Foxp3$^-$ T effector cells (T$_{eff}$), and CD3$^+$CD4$^+$Foxp3$^+$ regulatory T cells (T$_{reg}$). Myeloid cells were all pre-gated as $\gamma\delta$-TCR$^-$CD3$^-$ double negative and then gated as CD11c$^+$MHC-Class II$^+$ dendritic cells (DCs), Ly-6G$^+$CD11b$^+$ neutrophils (Neuts), and Ly-6G$^-$CD11b$^+$ClassII$^+$F4/80$^+$ macrophages (Macs). For nucleotide incorporation experiments, Click-iT® Plus EdU Flow Cytometry Assay Kits (Fisher) was used as per the manufacturer's protocol.

Histology

For histopathology, skin tissue was fixed in 10% formalin and paraffin-embedded, sectioned and stained with hematoxylin and eosin by the UCSF Mouse Pathology Core. Histopathology images were acquired on a Leica microscope using a DS-Ri1 camera and NIS-Elements software (Nikon). H&E quantifications of HF length, dermal infiltrate and epidermal hyperplasia were performed using ImageJ64 software (NIH, USA). For immunofluorescent tissue staining in Figure 1A, dorsal skin from Foxp3^{GFP} mice was first fixed in 2% PFA for 6-8 hr, washed with PBS and left in 30% sucrose overnight before embedding in OCT and freezing in a isopentane solution cooled over liquid nitrogen. 12ours, washed with PBS and left in 3SuperFrost slides (VWR), and stained with rabbit anti-GFP (Invitrogen, A11122) at 1:200 and chicken anti-Keratin-15 (Biolegend, Poly19339) at 1:400 or Rat anti-mouse/human ITGA6 (BD, 555734) at 1:300. Primary signal was amplified with Goat anti-Rabbit Alexa 488 and Goat anti-Chicken Alexa-555 or Goat anti-Rat Alexa-555 at 1:1000 (all from Invitrogen). Slides were then washed in PBS and mounted with DAPI containing medium. All images were acquired on a Zeiss Imager M2 fluorescent microscope with Apotome. Ki67 tissue staining was performed by the UCSF Dermatapathology Core using a Dako Link-48 stainer. Briefly, antigen retrieval was performed in Dako pH9 Retrieval Solution at 95°C for 1 hr and then stained with anti-Ki67 antibody (Dako, catalog # GA626) and the chromogen DAB. For detection, Dako Envision Dual Link was used. Finally, slides were counter-stained with hematoxylin.

In vivo Jag1 rescue

Foxp3^{DTR} mice depleted of T$_{regs}$ according to the early regimen were injected subcutaneously on days −2, −1, 1, and 3 into four adjacent dorsal skin sites with 1 μg control IgG1-Fc or Jag1-Fc fusion protein (both from R&D) conjugated to Affi-gel blue beads (100-200 mesh; Bio-Rad), as previously described (Chen et al., 2012). Briefly, per mouse: 1 μg of protein (in 10 μl) was soaked with 5 μL Affi-gel blue beads (corresponding to ∼2000 beads) for 1 hr at 37°C. Total suspensions of 15 μL were then transferred into 29G 3/10 cc insulin syringes (BD) for subcutaneous injection of mice under anesthesia. HFSC Ki67 expression was assessed by flow cytometry on day 4.

RNA-Sequencing analysis and Quantitative PCR

Sorted cell populations were flash frozen in liquid nitrogen and sent overnight on dry ice to Expression Analysis, Quintiles (Morrisville, NC). RNA samples were converted into cDNA libraries using the Illumina TruSeq Stranded mRNA sample preparation kit. (Illumina). RNA was isolated by Expression Analysis using QIAGEN RNeasy Spin Column and was quantified via Nanodrop ND-8000 spectrophotometer. RNA quality was checked by Agilent Bioanalyzer Pico Chip. cDNA was created from 220 pg of input RNA with the SMARTer Ultra Low input kit and sequenced to a 25M read depth with Illumina RNASeq. Reads were aligned to Ensembl mg GRCm38.p4 reference genome with TopHat software (v. 2.0.12). SAM files were generated with SAMtools from alignment results. Read counts were obtained with htseq-count (0.6.1p1) with the union option. Differential expression was determined using the R/Bioconductor package DESeq2 (Ref 2). Differentially expressed genes were analyzed by Ingenuity Pathway Analysis. Using the differentially expressed genes (p < 0.05) from the HFSC dataset, a python script was written to find the overlap between the DE list and known Notch target genes (Meier-Stiegen et al., 2010). To determine significance in overlap between the two, a chi-square

test was performed. The overlapping genes between the two sets were clustered in Cluster 3.0 and visualized as a heatmap using gene pattern's HierarchicalClusteringViewer (de Hoon et al., 2004; Reich et al., 2006). For assessment of differentiation associated genes in Foxp3$^{Cre/Cre}$Jag1$^{fl/fl}$ or control mice (i.e., Foxp3$^{Cre/Cre}$Jag1$^{wt/wt}$ or Foxp3$^{wt/wt}$Jag1$^{fl/fl}$), RNA was isolated from 1x10^6 epidermal cells on day 10 post depilation, using a column based kit (PureLink RNA Mini Kit, Thermo Fisher). For assessment of Jag1 expression on T cell subsets, T$_{regs}$, T$_{effs}$ and CD8$^+$ T cells were sorted from SDLNs of WT mice and RNA isolated as described above. RNA was then transcribed (iScript CDNA synthesis Kit, Bio-Rad) and the expression of differentiation genes or Jag1 for T cell subsets was assessed relative to Gapdh that was duplexed in every reaction. The following Taqman Gene expression assays were used (Thermo Fisher): Mm99999915_g1 (Gapdh), Mm01191753_m1 (Bgn), Mm00432359_m1 (Ccnd1), Mm01220860_m1 (Gdf10), Mm00486320_s1 (Sox4), Mm00776876_m1 (Sox7), Mm00441826_m1 (Timp3), and Mm00496902_m1 (Jag1). Data are presented as negative fold change of Delta-Delta CT or as standardized arbitrary units (AU).

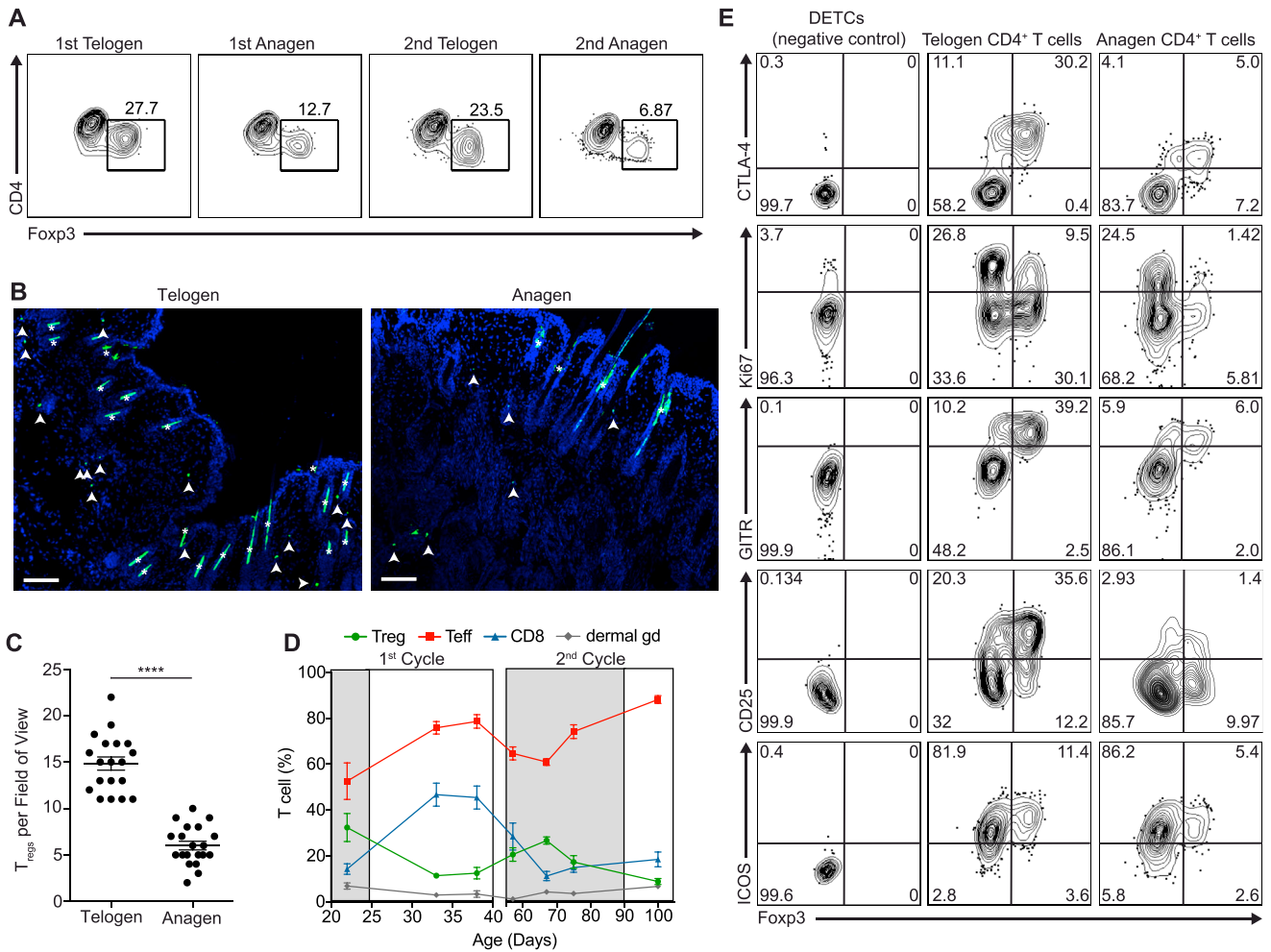### Intravital 2-photon imaging of T$_{regs}$ in dorsal skin

Two-photon imaging instrumentation has been previously described (Friedman et al., 2010). Dorsal hair of 7-10 week old Foxp3^{GFP} mice was clipped and depilated to induce anagen. Mice were then placed on a custom heated microscope stage under anesthesia. The custom suction window on the microscope stage was then placed into position over the depilated dorsum, and suction was applied to gently immobilize the depilated skin (Thornton et al., 2012). The microscope objective was then lowered into position directly over the suction window with an embedded 12 mm coverslip. 10 μg Evans Blue dye was injected into the retro-orbital vein immediately before image acquisition. All images were analyzed using Imaris Software (Bitplane). HFs were visualized using second harmonic generated collagen. Bulge-associated T$_{regs}$ were denoted as within a < 20 μm radius of individual HFs and non-bulge associated T$_{regs}$ as > 20 μm from a HF. To determine in vivo changes in T$_{reg}$ cell shape, the sphericity of individual T$_{regs}$ was calculated over the time-lapse period, as previously described (Thornton et al., 2012).

Statistical analyses

Statistical analyses were performed with Prism software package version 6.0 (GraphPad). *P* values were calculated using two-tailed unpaired or paired Student's t test. Sample size for animal experiments was determined based upon pilot experiments. Mice cohort size was designed to be sufficient to enable accurate determination of statistical significance. No animals were excluded from the statistical analysis, unless due to technical errors. Mice were randomly assigned to treatment or control groups, while ensuring inclusion criteria based on gender, age and hair cycle. Investigators were blinded for all tissue staining and clinical picture quantifications. Appropriate statistical analyses were applied, assuming a normal sample distribution. All in vivo experiments were conducted with at least two independent cohorts. RNA-Seq experiments were conducted using 2-4 biological samples (as indicated in figure legends) from indicated cohorts.

Data and Software Availability

RNA sequencing data has been deposited in NCBI with the following IDs: GEO: GSE76102 and GEO: GSE76138 and are available at: https://www.ncbi.nlm.nih.gov/geo/query/acc.cgi?acc=GSE76102 and https://www.ncbi.nlm.nih.gov/geo/query/acc.cgi?acc=GSE76138.

Figure S1. Skin-Resident Tregs Accumulate in Telogen Skin, Related to Figure 1

Treg cell abundance and activation in dorsal skin of adult wild-type (WT) C57BL/6 mice at specific stages of the synchronous HF cycle was assessed using flow cytometry. (A) Representative flow plots of skin Tregs profiled during the synchronous HF cycle. Pre-gated on live CD45+CD3+CD4+ cells. (B) Representative images of skin Tregs from dorsal skin harvested on post-natal day 21 (telogen) and post-natal day 30 (anagen). Arrows depict Foxp3+ Treg cells. Asterisks denote autofluorescent hair shafts. Scale Bars, 100 μm. (C) Quantification of absolute cell numbers of Foxp3+ Tregs per field of view in dorsal skin. (D) T cell subsets in dorsal skin of adult WT C57BL/6 mice. Data are shown as a proportion of CD3+ T cells. Shaded areas represent telogen phase and unshaded areas represent anagen phase. (E) Representative flow plots of negative control (dendritic epidermal T cells, DETCs) and CD4+ T cell gates from telogen and anagen dorsal skin. One representative experiment of two is shown (A); n = 3-5 mice per time point combined (C-D). Unpaired Students t test (C). ****p < 0.00., Data are mean ± s.e.m.
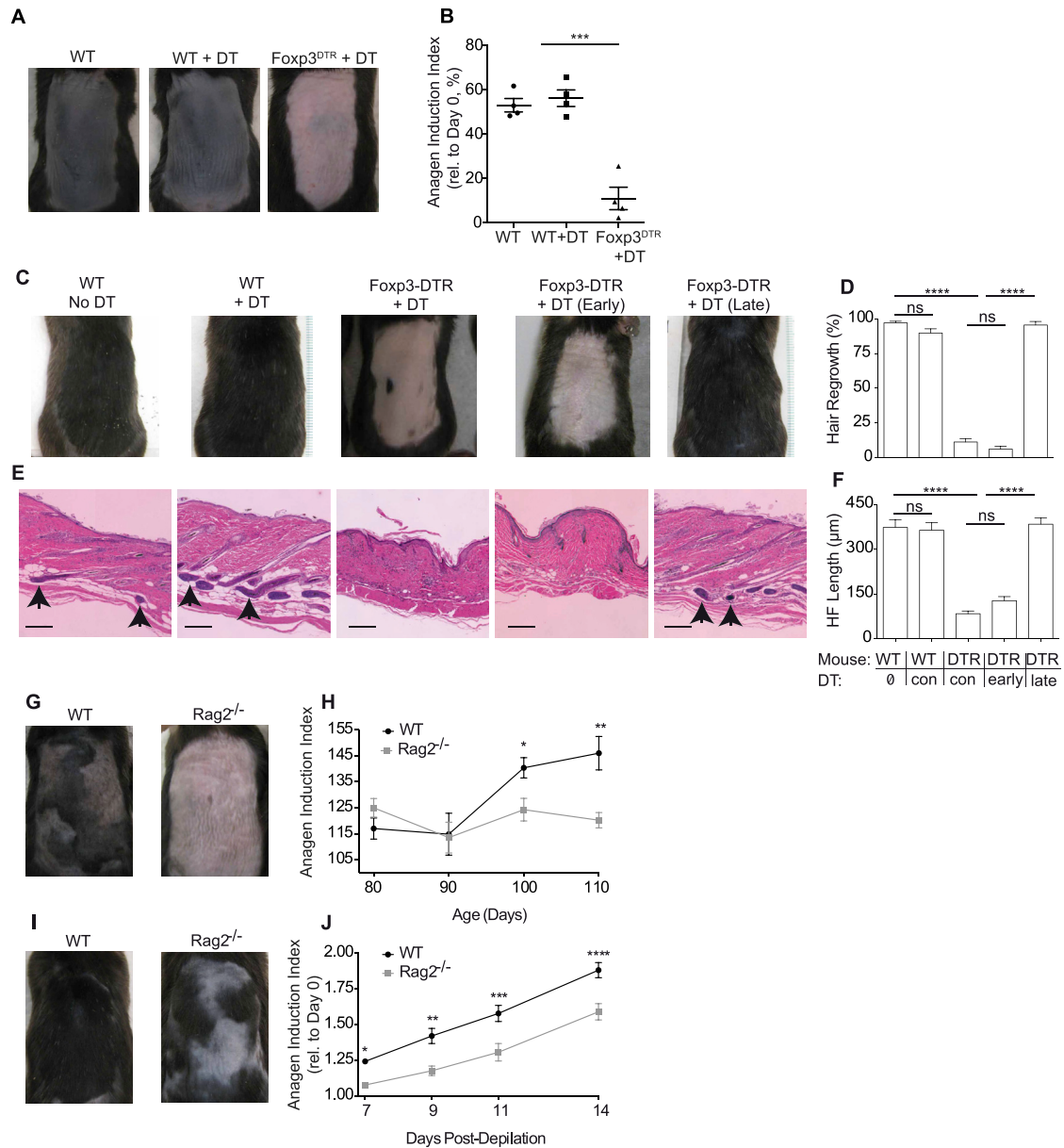
Figure S2. Tregs Are Required for Anagen Induction, Related to Figure 2

Control (WT) or Foxp3^{DTR} mice were treated with DT on days −2, −1, depilated on day 0 to induce anagen and DT administration continued on day 1 followed by every other day up to day 4. (A) Representative photos and (B) quantification of dorsal skin pigmentation at day 10 in WT and Foxp3^{DTR} mice with DT treatments as indicated. Tregs were depleted either up to day 4 (early), from day 7 onward (late) or constitutively (con) throughout the experimental period until the termination of the experiment at day 14. (C) Representative photos and (D) quantification of hair regrowth at day 14 in WT and Foxp3^{DTR} mice with DT treatments as indicated. (E) Representative H&E staining of skin from WT and Foxp3^{DTR} mice on day 14. Arrows indicate anagen HF extension into dermal adipose. (F) Quantification of HF length on day 14. WT and Rag2$^{−/−}$ mice were clinically assessed for spontaneous anagen induction during the natural HF cycle by monitoring skin pigmentation from 2nd telogen (Postnatal age of 80 days) through 2nd anagen (110 days of age). (G) Representative photos of WT and Rag2$^{−/−}$ mice at postnatal age of 110 days and (H) quantification of anagen induction by skin pigmentation intensity. WT and Rag2$^{−/−}$ mice with all dorsal HFs in 2nd telogen (Postnatal age of 80 days) were depilated to induce anagen. Anagen induction was monitored. (I) Representative photos in WT and Rag2$^{−/−}$ mice at 14 days post depilation and (J) quantification of anagen induction by skin pigmentation intensity analysis. One representative of three experiments shown. Scale Bars, 100 μm. n = 4-5 mice per group. One-way ANOVA (B, D, and F), Two-way ANOVA (H and J). ns = not significant, *p < 0.05, **p < 0.01 ***p < 0.001, ****p < 0.0001. Data are mean ± s.e.m.
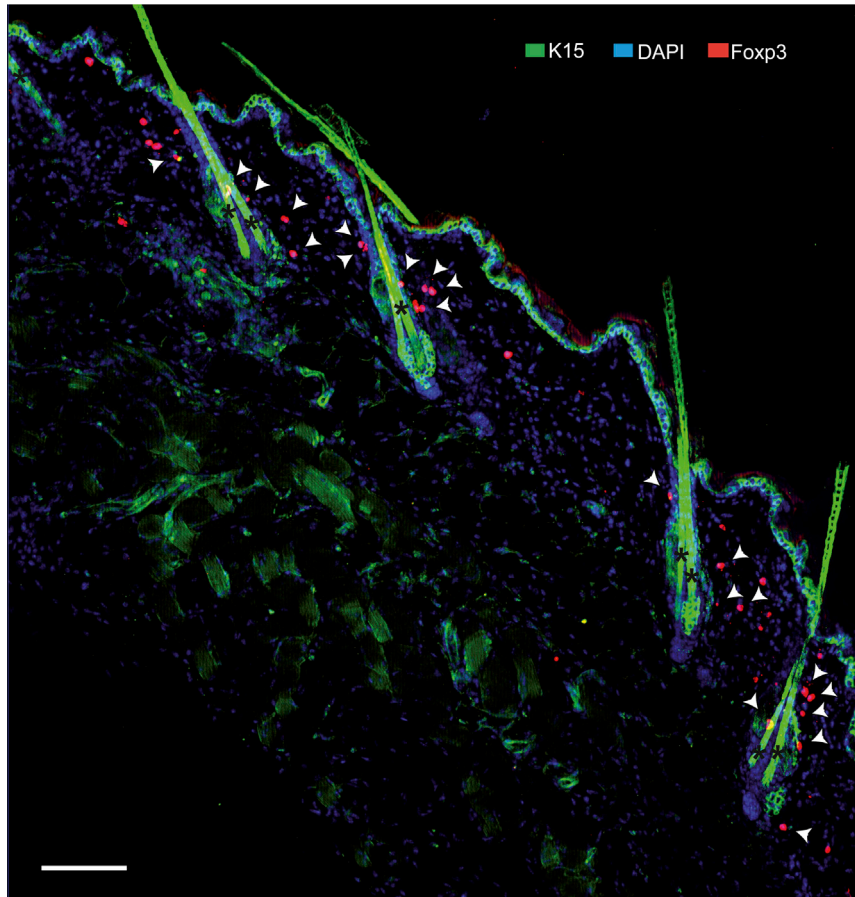
Figure S3. Tregs in Skin Preferentially Localize to Hair Follicles, Related to Figure 3

Representative immunofluorescent image of Foxp3^{+} Tregs in telogen skin of Foxp3[GFP] reporter mice co-stained with Keratin-15 (K15). Arrows depict Foxp3^{+} Treg cells. Asterisks denote autofluorescent hair shafts. Scale Bar, 100 μm.
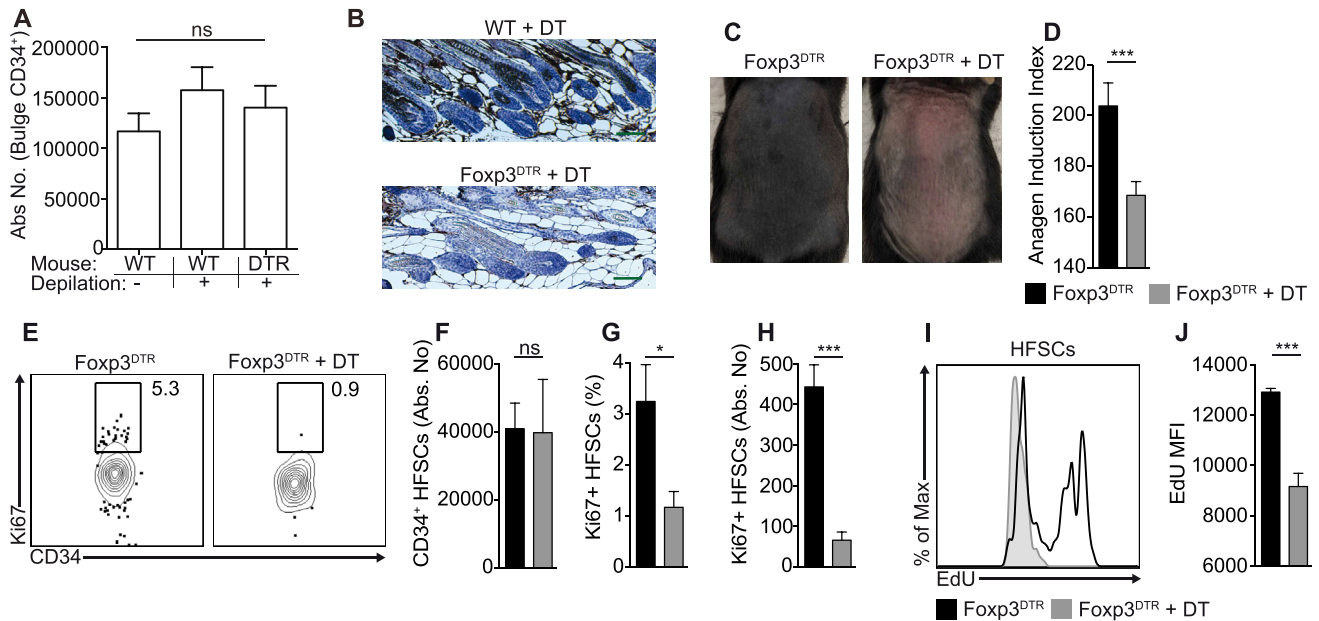
Figure S4. Tregs Play a Role in Promoting the Telogen-to-Anagen Transition during the Natural HF Cycle, Related to Figure 4

Foxp3^{DTR} or control mice were treated with DT on days -2, -1, depilated on day 0 to induce anagen and Diphtheria toxin (DT) administered again on days 1 and 3 (i.e., early regimen). (A) Quantification of total CD34$^+$ bulge HFSCs in WT and Foxp3^{DTR} mice 4 days after depilation. (B) Representative histological images of Ki67 staining of WT and Foxp3^{DTR} mice 10 days after depilation. Natural hair follicle cycle: DT or PBS (as control) was injected intraperitoneally into Foxp3^{DTR} mice to deplete Tregs during 1st telogen from postnatal day 21 (P21) to P24, and harvested at P32 for analysis. (C) Representative photos and (D) quantification of anagen induction in PBS treated (Foxp3^{DTR}) and DT treated (Foxp3^{DTR} + DT) mice. (E) Representative flow plots and quantification of (F) absolute number of HFSCs. Quantification of Ki67$^+$ HFSC (G) frequency and (H) absolute cell numbers. DT or PBS (as control) was injected intraperitoneally into Foxp3^{DTR} mice to deplete Tregs during 1st telogen from postnatal day 21 (P21) to P24. EdU (5-ethynyl-2′-deoxyuridine) was injected intraperitoneally at P31 and mice harvested at P32 for analysis. (I) Representative histogram plot of EdU staining from PBS treated (Foxp3^{DTR}) and DT treated (Foxp3^{DTR} + DT) mice. (J) Summary of median fluorescence intensity (MFI) of EdU expression. One representative experiment of three (A-B) and two (C-J) is shown. n = 4 mice per group. ns = no significant difference, One-way ANOVA (A), Unpaired Students t test (D, F-H, and J). *p < 0.05, ***p < 0.001, Data are mean ± s.e.m.
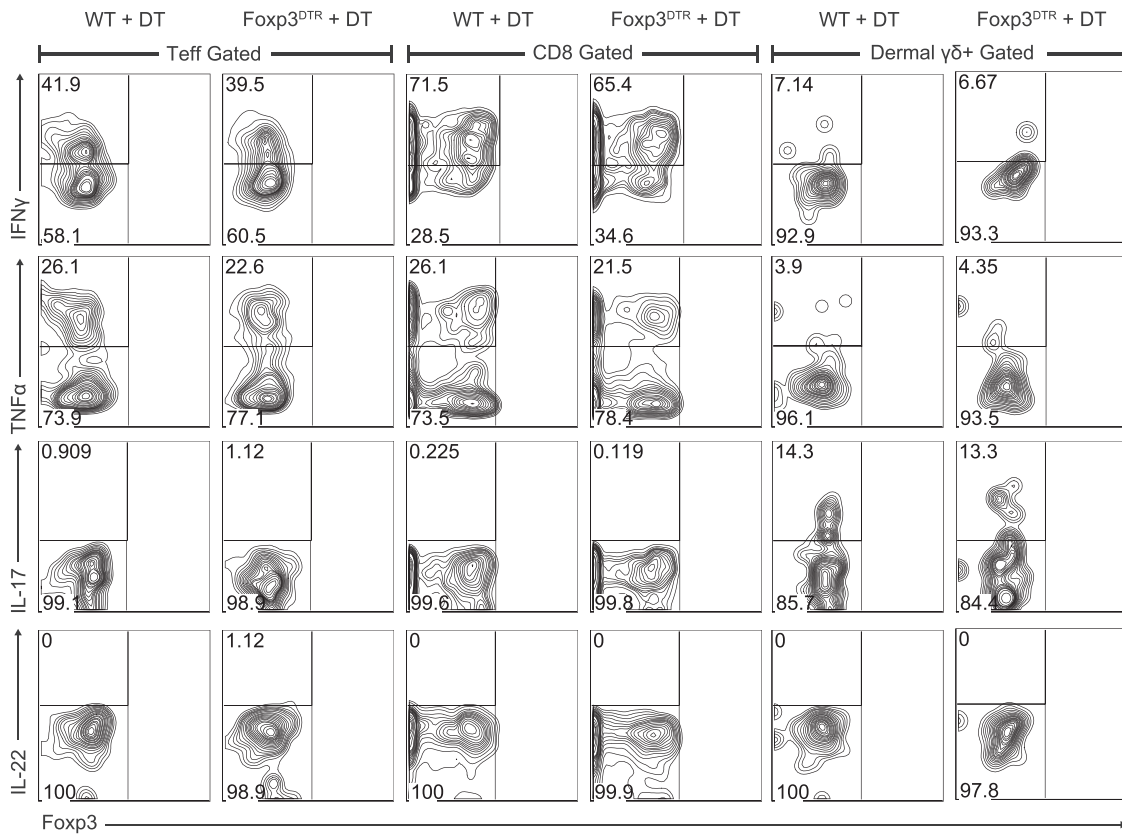
Figure S5. Transient Treg Loss Results in Minimal Skin Inflammation, Related to Figure 5

Control wild-type (WT) or Foxp3^{DTR} mice were depilated and treated with DT according to the 'early' depletion protocol. Single cell suspensions from day 1 skin were stimulated with PMA/ionomycin and the production of IL-22, IFNg, IL-17 and TNF-alpha was assessed by flow cytometry. Representative flow cytometry plots of cytokine induction are shown. One representative experiment of two; n = 3-5 mice per group.
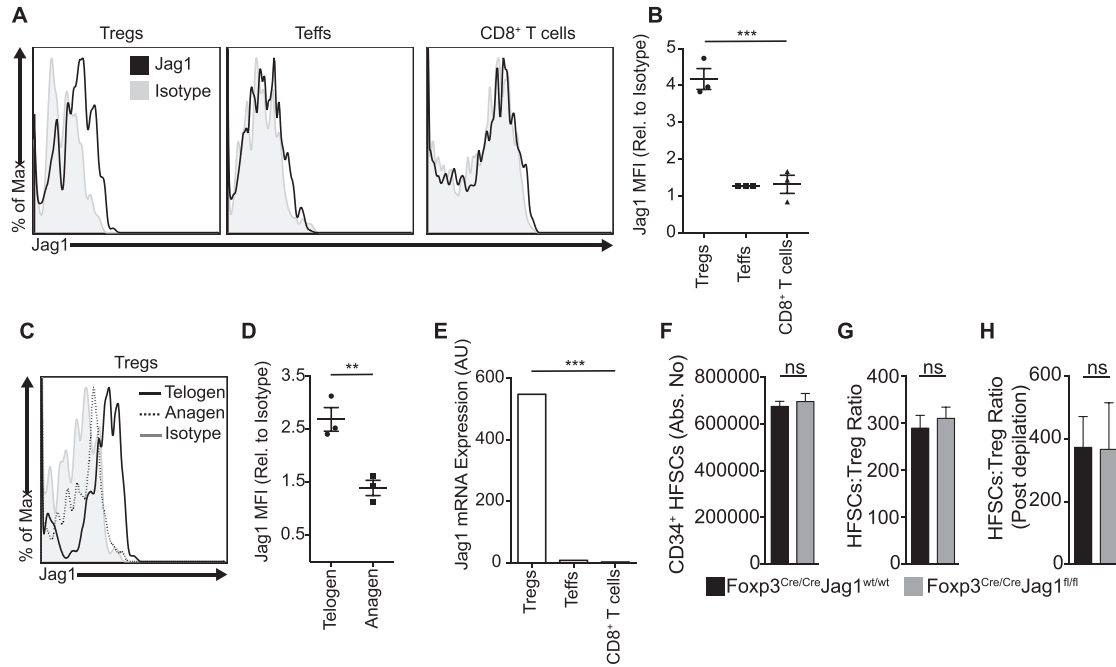
Figure S6. Tregs Preferentially Express Jagged 1, Related to Figure 6

T cell subsets from wild-type C57BL/6 mice were assessed for Jag1 expression by flow cytometry. (A) Representative histogram plots of isotype staining and Jag1 staining from indicated T cell populations. (B) Summary of median fluorescence intensity (MFI) of Jag1 expression relative to isotype control MFI. (C) Representative histogram plots of isotype and Jag1 staining of telogen and anagen skin resident Tregs. (D) Summary of Jag1 MFI expression relative to isotype control. (E) Jag1 expression via qRT-PCR, expressed in arbitrary units (AU) for all populations tested. Quantification of (F) total bulge HFSCs and (G) HFSC:Treg ratio in control (Foxp3$^{Cre/Cre}$Jag1$^{wt/wt}$) or Treg-Jag1 deleted mice (Foxp3$^{Cre/Cre}$Jag1$^{fl/fl}$) in steady state non-depilated skin of 8 week old mice. (H) HFSC:Treg ratio assessed on day 10 post depilation. One representative experiment of two is shown. One-way ANOVA (B and E), Unpaired Student's t test (D, F-H). n = 3-5 mice per group. ns = no significant difference, **p < 0.01, ***p < 0.001, Data are mean ± s.e.m.